CHALMERS

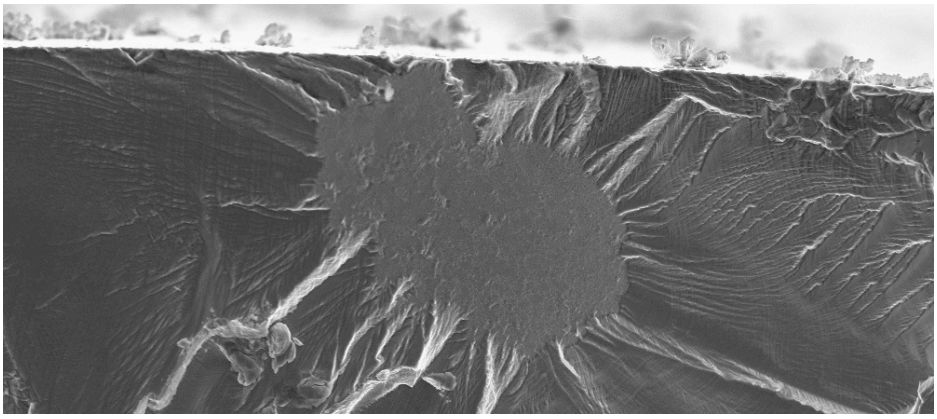

Fatigue Initiation Fail Mode Classification of a Nickel-base Superalloy

Master's Thesis in Applied Physics

STEFAN FORSMAN

Department of Applied Physics
Microscopy and Microanalysis
Chalmers University of Technology
Gothenburg, Sweden 2012

Master's Thesis 2012

THESIS FOR THE DEGREE OF MASTER OF SCIENCE

Fatigue Initiation Fail Mode Classification of a Nickel-base Superalloy

STEFAN FORSMAN

CHALMERS

Department of Applied Physics
Microscopy and Microanalysis
CHALMERS UNIVERSITY OF TECHNOLOGY
Gotheburg, Sweden 2012

Fatigue Initiation Fail Mode Classification of a Nickel-base Superalloy

STEFAN FORSMAN

Department of Applied Physics Microscopy and Microanalysis
Chalmers University of Technology
SE-412 96 Göteborg, Sweden
Telephone +46(0)31-772 1000

Printed at Chalmers Reproservice
Göteborg, 2012

Cover illustration: *A fractograph showing a surface initiation in a sample tested at 650° C.*

Abstract

Inconel-718 is a nickel-base superalloy frequently used in aircraft engines and land-based turbines for its high-temperature and corrosion resistance. In this work a large number of fracture surfaces from fatigue specimens of Inconel-718 have been studied with the main purpose to identify and learn more of initiation mechanisms acting in this specific alloy. Initiation sites have been identified, measured by size and investigated using SEM in an attempt to determine the cause of crack initiation. Specifically the impact of casting defects was of interest. It has been found that facets are the primary initiation points for cracks at RT and 650°C and not large defects such as pores or inclusions, two internal initiations found was connected to embrittlement through laves phase. Surface initiations are in the size range of ∼40-170 μm, this size was approximated to a good degree by Kitagawa-Takahashi diagrams that gave an average maximum defect size of 190 μm.

Acknowledgements

I would like to extend my gratitude first and foremost to Volvo Aero Corporation and its employees for making this work possible. A special thanks to my supervisors Thomas Hansson at Volvo Aero and Krystyna Stiller at Chalmers for guidance and fruitful discussions. I would also like to thank Kenneth Andersson and Björn Karlsson for guidance in the world of fractography as well as Magnus Hörnqvist, Peter Georgsson and Tomas Månsson for generally interesting input to my work. Thanks also to everyone else at the materials department for answering any questions that was on my mind.

Stefan Forsman, Trollhättan 12/06/15

Contents

1 Introduction

Fatigue is a failure mechanism in materials that occur from cyclic loading of components. Research regarding fatigue has been performed since the middle of the 19th century and is today an established engineering tool [1]. The relationship to fatigue analysis in safe life applications, such as aero applications where a failure must be guaranteed not to occur, is somewhat special. In these applications a components life is calculated from a minimum life point of view. Designing this way will naturally be a bit of a dilemma for engineers. If a component is calculated to have a longer life than the actual accidents may occur, risking the lives of many people. On the other hand if a component is calculated to have a much too short life than the actual it may lead to waste of both human and material resources. Conservative life calculations could lead to both excessive engine inspections, wasting human labour, and scrapping of perfectly sound components. It is therefore essential that evaluation of life data is based on theories formulated through thorough research.

1.1 Background

In jet engines a range of different materials and manufacture methods are used in the production of components. In cold parts of the engine titanium alloys are used extensively due to their high strength to lightweight properties, while hot sections are dominated by superalloys with high temperature strength properties. Volvo Aero is an aerospace company with a history of producing the swedish military aircraft and is a part of the Volvo Group company. In later years the market for development and production of military aircraft engines have stagnated and focus has changed to development and production of civil aircraft engine components. In the civil market focus has been production of large and advanced structural components, so called load carrying structures. In hot sections of the engine these parts are typically cast, due to their complex geometry and moderate demand for strength. Compared to forging casting is a cheaper and easier way to manufacture metal components of complex geometry, but one of the major drawbacks is the lowered fatigue properties. The life of cast components is not only shortened but also more difficult to predict when compared to a forged component manufactured from the same material. The lowered fatigue properties are explained by the large grain size, material inhomogeneity and existence of casting defects [2][3].

Casting defects have a large influence on the fatigue properties of components. A large defect will quickly initiate a crack which could be very detri-

mental to the total life, i.e amount of cycles to failure. Large defects are of course not acceptable in manufactured components that are to be used for aerospace applications; therefore all components are subject to Non-Destructive Testing (NDT). At Volvo Aero radiographic investigations are performed to discover defects in cast components, samples for mechanical testing are also exposed to similar investigations.

Radiographic investigations are however not completely reliable, there is a limit to how small defects may be found and distribution of defects may also have an effect on chance of discovery; discovery of defects depend on that the signal from defect material deviate from non-defect material, if defects are evenly distributed in the component discovery is more difficult [4]. Destructive testing (DT) may also be used to determine the defect distribution. In a recent study the use of Very-High Cycle Fatigue (VHCF) have been used to estimate the distribution of defects in high-performance steel [5].

1.2 Aim

Casting defects reduce fatigue life due to that they serve as sites of crack initiation. By studying fracture surfaces of fatigue samples the crack initiation sites can be found and the cause of initiation determined, in this way the defects undetected by radiographic investigations can be found. The aim of this study has been to determine the effect these defects have on fatigue life in a nickel base superalloy used in aerospace applications.

A secondary objective has been to investigate if different failure mechanisms are favored depending on external parameters, such as temperature and stress/strain range.

1.3 Purpose

Several studies performed argue for a new safe life fatigue evaluation method [6][7], where fatigue failure is seen as a competition between different failure mechanisms. If it is assumed that every mechanism has a mean and minimum failure life a safe life evaluation need only consider the mechanisms with minimum failure life. The purpose of this study has been to investigate and gain a better understanding of how large the impact of casting defects are in fatigue life of a nickel base superalloy. If a life limiting failure mechanism is found it could be used to improve the safe life evaluation of the specific material. An investigation of this kind is also of educational importance to the organization.

Figure 1: *A picture of a typical LCF sample.*

Last but not least an investigation such as this will serve as a quality check of the material in question. This is of major importance when choosing which fatigue evaluation approach that is best suited for life calculations. In a material where large defects are common the material must be considered to be pre-cracked and life will be governed by crack propagation. In a "clean", defect free, material crack initiation must also be considered.

1.4 Method

In order to evaluate fatigue properties of different materials at VAC, extensive testing has been performed in both Low-Cycle Fatigue (LCF) and High-Cycle Fatigue (HCF) regions, a fractured smooth LCF sample is seen in Figure 1. The fracture surfaces of these smooth samples has been subject to fractographic investigation by optical microscope (OM) and Scanning Electron Microscope (SEM). The crack initiation site has been located and classified depending on what kind of failure mechanism initiated the crack; the size of the initiation sites have also been measured. Using crack propagation models, which take this initial crack size as input parameter, the propagation life of each sample has been calculated and compared to the measured (total) actual life. This comparison can be used to determine an approximate crack initiation life as total life minus calculated propagation life.

Notched samples have been investigated in order to understand if the initiation behavior is similar for notched and smooth samples. In a smooth sample the area where a fatigue crack may be initiated is large, by notching

the sample and reducing the load this area is effectively reduced. If initiation is caused by a defect in smooth samples and this defect is also found to initiate notched samples the conclusion that the defect is very common may be drawn.

1.5 Limitations

The first and most important limitation is that only one material will be investigated. A number of different materials are used by Volvo Aero but it is very likely that different materials have different distributions of casting defects and that fatigue properties are affected differently by them. Investigating one material is thus a very reasonable limitation.

For the specific material there are many different samples to investigate. In order to keep the amount of parameters on a reasonable level smooth samples tested at two different temperatures will be investigated, room temperature (RT) and high temperature 650°C. This selection will make it possible to investigate the effect of temperature without consuming too much time by investigating samples at several different temperatures. Notched samples have been tested at 550°C.

A selection has also been done concerning stress/strain ranges. Focus has been to investigate samples that have been tested at low stress/strain due to the increased chance of crack initiation at large defects compared to higher stress/strain [5]. As stress/strain is increased the amount of initiation sites increase and it also becomes more difficult to classify them.

1.6 Report structure

The report following this section starts with a Literature study section, here basic knowledge of fatigue testing and fatigue data evaluation is presented for the reader unfamiliar with this subject. If this subject is well known to the reader these two subsections may be skipped. This is followed by a description of the mechanisms that initiate and propagate fatigue cracks, fatigue fracture surface characteristics and theories regarding casting defects. These subsections contain both general well known theories and previous work of more specific interest to this report.

The literature study section is followed by a method section, Numerical calculations, that in more detail explains the numerical calculations. In the Results section all results from fractographic investigations are presented with images and interpretations of said images. The crack propagation life

calculated using fracture mechanics is also compared to the real fatigue life. These results are later discussed in the Discussion section, the discoveries are here related to previous work in an attempt to explain features that appear on fractographs and relationships between these features and fatigue life. The conclusions of the report regarding results and possible future work is summarized in the Conclusions section of the report.

2 Literature Study

2.1 Superalloy Inconel-718

The environment inside the hottest parts of a jet engine is extreme, materials used in these regions needs to sustain their properties at high temperatures and be highly resistant to corrosive agents. The term superalloy was coined during the development of materials specifically designed for use in such extreme environments. Today they are still mainly used in aero and space applications, but also find an increasing application in land-based turbines for generation of electricity [8].

The material investigated in this report is cast Inconel-718, a nickel-base superalloy. The alloy contains mainly five elements, nickel ∼50 %, Chromium ∼20 %, Iron ∼17 %, Niobium ∼4.75 % and Molybdenum ∼2.8 % as well as small parts Titanium, Aluminum, Cobalt, Silicon and Manganese. The alloy may contain some other elements as well but they constitute a very small part of the material. The material is used in the temperature range of -250°C to 700°C and mainly finds its application is structural components, such as casings, in jet engines and land based turbines [9].

2.2 Fatigue testing

The basics of fatigue testing are quite easily grasped if one does not go too much into detail. Fatigue testing may be divided into two types. The purpose of the first type of fatigue testing is to measure the total fatigue life. A sample is exposed to cyclic loads at a predetermined magnitude, either load or strain dependent, the samples are run until they fracture or when a specific crack size is reached. The number of cycles until failure are then recorded. Typically a few samples are run at every investigated cyclic load to get an accurate value of standard deviation.

In the second type the purpose is to measure the rate of crack growth depending on crack size and stress. In order to measure the crack growth a sample containing a crack is needed. This is typically done by notching a sample and exposing it to cyclic loads until a crack of appropriate size is created. Electrodes are then mounted on the sample, after calibration the potential drop can be used to measure the crack size, and the sample is once again exposed to cyclic loads. The crack size is measured every tenth cycle and the crack growth rate is calculated from these values. Details about parameters and models used in the evaluation of fatigue testing is further presented in section 2.3.

An important parameter when it comes to stress controlled fatigue testing is the R-value which is defined as

$$R = \frac{\sigma_{min}}{\sigma_{max}}, \tag{1}$$

where σ_{min} is the minimum stress during a cycle and σ_{max} is the maximum stress during a cycle. A typical value for fatigue testing is $R = 0$, where a cycle consists of applying a tensile load corresponding to σ_{max} followed by relaxation of the sample back to its initial position, thus $\sigma_{min} = 0$, unless plastic strains are involved. To be able to calculate an accurate fatigue life for a component in service it is important that the R-value while testing corresponds to the real loads the component is exposed to, since the fatigue life varies much depending on this parameter. In the interval $R \in [-1,1[$ it can generally be said that higher R-value corresponds to a shorter life for a given stress/strain range. For strain controlled testing the R-value used is generally R_ϵ, defined through strain rather than stress as

$$R_\epsilon = \frac{\epsilon_{min}}{\epsilon_{max}} \tag{2}$$

2.3 Fatigue evaluation

There are quite a few ways to evaluate fatigue data from testing but the basic question one wants answered is always the same. What is the expected fatigue life of a component when exposed to a specific environment? Regrettably there is no single method that covers all cases, different materials and situations require different evaluation methods. Fundamentals of metal fatigue analysis by Bannantine, Comer and Handrock covers the three most fundamental evaluation methods that will be discussed in this section [1].

2.3.1 Stress-Life

During the years of fatigue research it has shown that the most important parameter that decides fatigue life is not maximum or minimum stress in cycles but the total stress range $\Delta\sigma$, defined as

$$\Delta\sigma = \sigma_{max} - \sigma_{min}. \tag{3}$$

The relationship between fatigue life N and stress range $\Delta\sigma$ is exponential and can be expressed as $\Delta\sigma = A \cdot N^c$. In order to acquire fatigue life for any stress range within the tested interval, data from testing is used to fit the coefficients A and c.

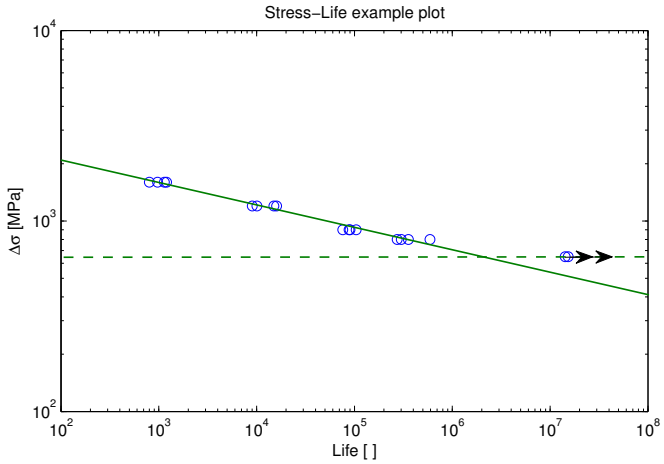

Figure 2: *A typical idealized Stress-Life plot, dashed line is the fatigue limit, arrows indicate run-out samples. The linear approximation in the log-log scale is a good approximation until the fatigue limit is reached, below this limit stresses are not high enough to initiate and/or propagate a crack and thus failure does not occur.*

Test data plotted as $\log(N)$ vs $\log(\Delta\sigma)$ together with a fitted curve will typically look as in Figure 2. The exponential relationship is obviously a good approximation but for lower stress ranges the approximation breaks down as the life of tested samples diverges toward infinite life. The point where life diverges toward infinity is called the fatigue limit; the fatigue limit is the maximum stress for which a material has infinite life. It is quite expected that such a limit should exist but surprisingly not all materials have one, aluminum is such an example.

The stress-life method is probably the simplest method of evaluating fatigue life but it has shown that it is only valid in cases where the response of the material towards the applied cyclic loads is elastic. Fatigue testing where no plastic strains are involved is often referred to as High-cycle fatigue (HCF) testing as opposed to Low-cycle fatigue (LCF) testing. If plastic strains are involved the relationship between stress range and life breaks down and becomes a bad approximation. In order to evaluate fatigue data at higher stresses where plastic strains are inevitable the strain-life method may be applied.

2.3.2 Strain-Life

The strain-life approach is based on the observation that fatigue life is strain dependent; the advantage with this approach is that the model is accu-

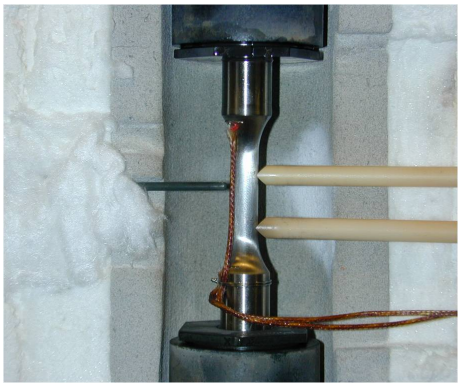

Figure 3: *A picture showing the typical rigging of a fatigue sample where strain dependent loads are cycled. The strain is measured in the zone between the two white rods, thermocouples are also present here to control temperature.*

rate even at high loads where plastic strains are nonzero. Considering that stresses and strains are linearly dependent through Hooke's law when plastic deformations are close to zero, strain-life and stress-life methods are equivalent in this range. The reason for not always using the strain-life over stress-life method is that it is a bit more cumbersome. It is a lot easier to cycle a load dependent sample compared to a strain dependent. In a load controlled machine you need only make sure you apply the same load each cycle, to get an accurate measurement in a strain controlled cycle you must measure the strain directly in the deformation zone of your sample. The rigging required of a sample is seen in Figure 3.

Analogous to the stress-life approach it is the strain range

$$\Delta\epsilon = \epsilon_{max} - \epsilon_{min} \tag{4}$$

that is the important parameter when evaluating fatigue life. Common is to fit a Coffin-Manson-Basquin curve to the data points according to

$$\frac{\Delta\epsilon}{2} = A \cdot (2N)^b + B \cdot (2N)^c, \tag{5}$$

where A, b, B and c are fitted coefficients. This function is a sum of two exponential functions, the first corresponds to the elastic strain and the second to the plastic strain. If both plastic and elastic strains are measured during testing the two terms can be fitted separately using linear regression.

2.3.3 Fracture mechanics

A third much used way of evaluating fatigue life of components is based on fracture mechanics. It differs from the stress- and strain-life methods in

that measurements are not focused on measuring the total life of a specific material at a specific stress/strain range, but rather to measure the rate of crack growth. Fracture mechanics is useful when dealing with materials or structures that are known to have small cracks or imperfections even before they are exposed to cyclic loads. Materials containing casting defects, inclusions or welded material are such examples. When evaluating life it is assumed that a crack of a specific size exists within the structure from the beginning. Using the crack growth rate known from testing the remaining life of the component can be determined. In aircraft engine applications fracture mechanics is also used when determining the periodicity between engine inspections. During inspection engineers look for small cracks on the surface, knowing the size of the smallest crack they can discover they can calculate the time it will take for such a crack to grow to a dangerous size. Inspection times are then set to be shorter than this time period, which guarantees that no failure will occur in between.

What decides the rate of crack growth is the stress intensity factor K, that is the magnitude of the local stress in the vicinity of the crack front. Due to the crack this local stress will be amplified compared to the global stress in the sample. In Fracture mechanics generally three modes of loading, which leads to different crack surface displacements, are discussed. Mode I, II and III.

Mode I Tensile mode (crack faces pulled apart)

Mode II In-plane shear (crack faces slide over each other)

Mode III Anti-plane shear (crack faces slide relative to each other, perpendicularly to the crack growth direction)

In this report Mode I only is regarded, since this is the loading mode used for testing, thus henceforth $K = K_I$. K depends on a number of different parameters where crack size, crack shape, sample geometry and of course stress are most important. The general form is given by

$$K = f(g)\sigma\sqrt{\pi a}, \tag{6}$$

where $f(g)$ is a factor that depends on the crack shape and sample geometry, a is the crack length and σ is the applied global stress in the sample. In cyclic loads the stress range is the important parameter and it has been found that crack growth rate depends on a stress intensity factor range ΔK, evaluated as

$$\Delta K = K_{max} - K_{min} = f(g)\Delta\sigma\sqrt{\pi a}. \tag{7}$$

As described in the section above crack growth testing is conducted through measuring the crack size a as a function of cycle number N. From this curve

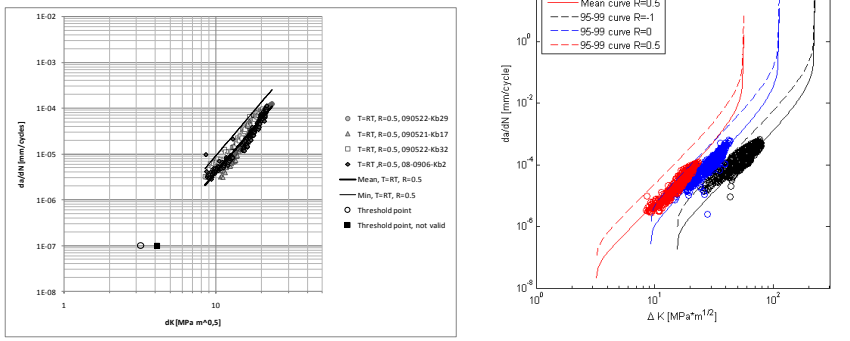

(a) Paris' law (b) Complete crack growth rate curve

Figure 4: ***a)*** *A plot showing the fitting of a curve according to Paris' law which is valid for intermediate values of* ΔK*. Measured threshold values are also included in this plot as well as a min crack propagation curve created from shifting of the mean curve.* ***b)*** *A plot showing a complete crack growth rate curve for three different R-values, the curve diverges toward a crack growth rate of zero near* ΔK_{th} *and towards an infinite value near* K_c*.*

a numerical derivative of crack growth rate $\frac{da}{dN}$ is calculated. Data points of $\frac{da}{dN}$ is then plotted against ΔK, which are calculated for the corresponding crack size and specific stress range. These data points are then fitted to a curve, the most widely accepted being the Paris' law according to

$$\frac{da}{dN} = C(\Delta K)^m, \tag{8}$$

where C and m are material constants fitted using linear regression. This curve will form a straight line in a log-log diagram, an example of fitting can be seen in Figure 4(a).

The Paris' law is only valid for a specific interval of ΔK. For lower values of ΔK the curve diverges toward a crack growth rate of zero which is reached at ΔK_{th}, a threshold value of crack growth. In the same way the curve diverges toward infinite values of crack growth rate for a critical stress intensity K_c. Often an accurate complete curve requires specific measurements of threshold value, the value of critical stress intensity does not significantly affect the total crack propagation life and is not as important. A complete crack growth rate curve created by combining two different measurements can be seen in Figure 4(b).

NASGRO, the crack propagation analysis tool used at Volvo Aero, uses the

following NASGRO equation to fit complete crack growth rate curves

$$\frac{da}{dN} = C\left(\left(\frac{1-f}{1-R}\right)\Delta K\right)^n \frac{\left(1-\frac{\Delta K_{th}}{\Delta K}\right)^p}{\left(1-\frac{K_{max}}{K_c}\right)^q}, \tag{9}$$

where f is the crack opening function and C,n, p, q are empirically derived constants [10]. The model is a modification of Paris' law that applies near critical and threshold values of the stress intensity factor range ΔK. This model also includes the R-ratio as a parameter and it can thus be used to approximate crack propagation for values of R that has not been explicitly tested.

As mentioned above the drawback of this approach is the requirement that an initial crack size must be known (or accurately approximated) in order to calculate an accurate life. Using fracture mechanics we may calculate the crack propagation but not crack initiation times. Crack initiation may however be calculated when combining fracture mechanics with stress/strain-life testing and fractographic investigations. A fractographic investigation may give an approximate size of the crack where crack propagation started; this value may then be used with fracture mechanics to calculate a propagation life. The initiation life is then given simply as total life minus the calculated propagation life. If this value is found to be close to zero the conclusion that some kind of defect initiated the crack may be drawn.

2.4 Crack initiation & propagation

Fatigue fracture of components may occur at very low stresses where the response of metals towards applied loads is considered to be elastic. In the macroscopic sense this elastic approximation is absolutely true for a single cycle, but locally some small deformation must occur with each load or fatigue would not exist. These deformations, although small, add up with each cycle until failure.

Early on the cause for fatigue of metals was connected to the initiation and propagation of cracks. In 1903 Ewing and Humphrey used an optical microscope to observe the creation of slip-lines in the crystal structure of iron after a few cycles of loading. When the same area was investigated once again after another set of applied cyclic loads the lines had broadened. This process of broadening continued as more cycles was applied until the so called slip bands started to crack. What Ewing and Humphrey had discovered was what is today referred to as Stage 1 fatigue, crack initiation. The initiation of cracks is followed by crack propagation, Stage 2 fatigue. Both kinds are illustrated in Figure 5. Stage II fatigue commences where the

crack grows perpendicularly to the load direction. The crack will propagate with each cycle until a critical crack size is reached and fracture occurs.

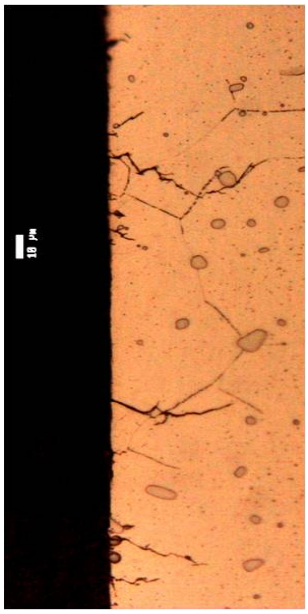

Figure 5: *A picture showing a polished cross section of a surface crack initiation. The load direction is vertical.*

2.4.1 Near perfect metal

The ideal crack initiation in a near perfect metal without cracks or other defects starts with the slipping between crystallographic planes within a single grain at the surface of the material [11]. Creation of these so called persistent slip bands start at the surface due to that the grains are not as confined here as within the material, there is simply more room for deformations to occur. A perfect crystallographic plane is of course not easily slipped, the reason that planes may slip at even low elastic stresses are due to dislocations in the material that make some planes move more easily [11]. The effect dislocations have is schematically exemplified in Figure 6. In this Figure we see an edge dislocation that, if moved to the edge of the crystal, will appear as if the whole plane has slipped one step. Compared to a perfectly crystalline plane a dislocation plane will slip more easily simply because moving the dislocation is enough to cause slip. Moving the dislocation requires the breaking of one atomic bond at a time, while slipping a perfect crystal plane requires all atomic bonds in the plane to be broken at the same time. Internal stresses in the material may also contribute to the

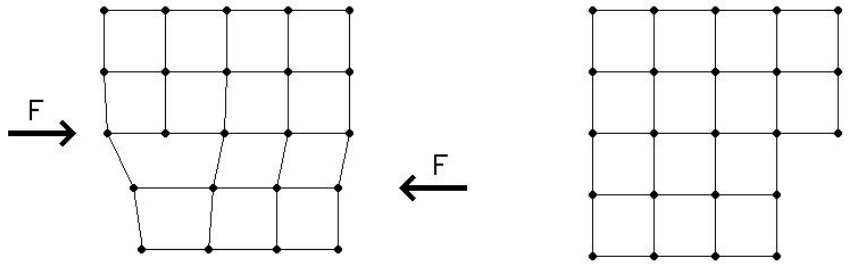

Figure 6: *A schematic image showing how an edge dislocation may weaken a slip plane.*

deformation of slip planes at low external stresses.

The slipping occurs in grains that have their weakest slip directions parallel to the direction of maximum shear at a 45° angle towards the fracture plane, which is perpendicular to the load direction. Of course not every grain in the metal will fulfill the specific conditions of dislocation distribution and plane alignment, but with the numerous amounts of grains at the surface there will always be several who do, see Figure 7(a).

How cracks are formed from the back and forth slipping of planes is illustrated in Figure 7(b). The situation is somewhat similar to a stacked deck of cards, by moving the uppermost card back and forth the other cards will also move in a random fashion. Due to hardening or softening effects, making planes that slip become less/more prone to slip again, this movement is not random in crystal planes. Extrusions and intrusions are formed in this process and dislocations are stacked up leading to stress concentrations. Grain size has a large influence on this mechanism. A large grain size will allow long slip-planes and stacking of many dislocations leading to high stress concentrations. This increased local stress will affect the neighboring grain when creation of slip-planes has continued long enough. The slip-plane process may be transferred to this grain if conditions considering plane alignment and dislocation distribution are met or the grain boundary may be cracked if the local stresses are high enough.

No well-recognized definition of when crack initiation transcends into crack propagation exists. Sometimes it is defined as when the crack has attained a specific length (1 mm, 1 μm) or comparable in length to a few grain sizes [12]. But as the local deformation grows it will at some point act more as a crack than a collection of slip-bands, this means that the process changes from initiation to propagation and can be noticed by that the crack growth

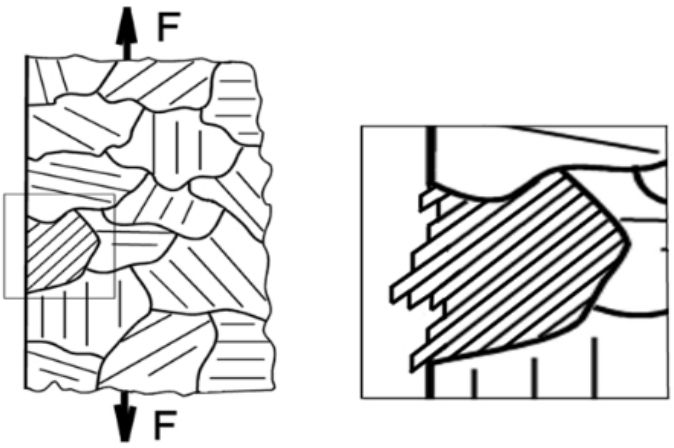

(a) Crystal plane orientation (b) Surface grain

Figure 7: ***a)*** *An image showing the orientation of potential crystallographic slip planes in surface grains* ***b)*** *A surface grain with suitably oriented crystallographic planes, extrusions and intrusions have formed after several applied cyclic loads. Note that each layer in this image represents several crystal planes.*

changes direction. Instead of growing in the direction of maximum shear the crack tends to grow perpendicular to the direction of applied stress, so called stage II fatigue [13].

Stage II fatigue, or crack propagation, is characterized by the formation of striations on the fatigue surface. Striations have an appearance similar to the rings created in growing trees, each striation corresponds to the position of the crack front during one cycle and thus the distance between striations correspond to the crack growth for one cycle. Typical striations can be seen in Figure 8. The striations in this figure were created when the propagating crack was very large and the sample near failure, the distance between striations is $\sim 10\ \mu m$.

Some different models for striation formation exists, a model for sawtooth striation formation is illustrated in Figure 9. During the tensile part of a cycle material separates at the very edge of the crack front. The opened crack is plastically deformed during the compressive part of the cycle which forms the tooth pattern that shows when the crack opens up during the next tensile load.

Striations are most interesting when performing a fractographic investigation of structural components that have failed in service. In such cases the reason for failure is often unknown, striations are characteristic for fatigue failure and thus if they are found the conclusion that fatigue was involved in the failure can be drawn. Information regarding loading history during

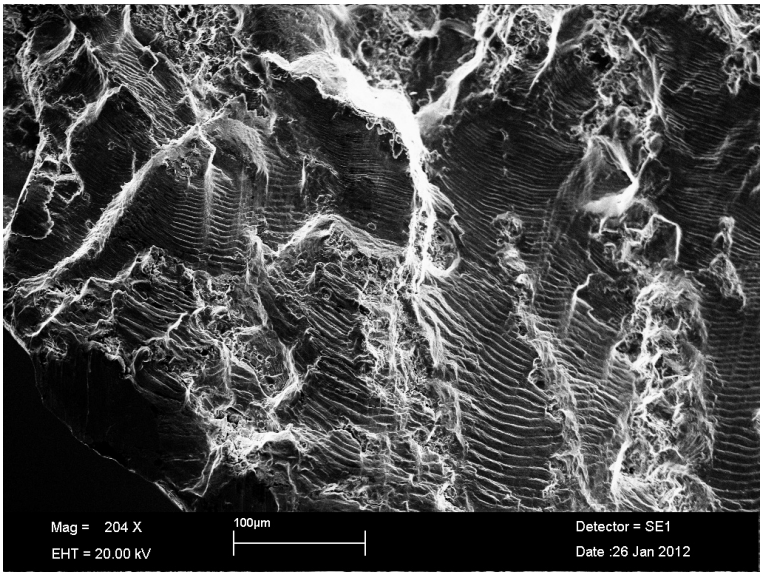

Figure 8: *A picture showing a typical example of fatigue striations*

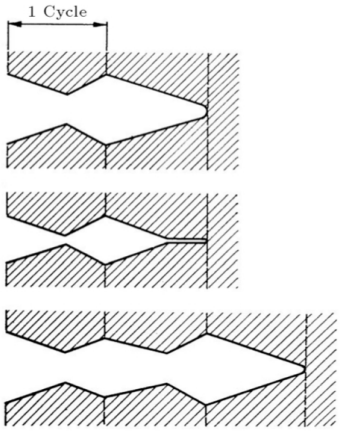

Figure 9: *Schematic illustration of sawtooth striation formation during fatigue. First step is after tensile loading. Second step is after the tensile load has been replaced by a compressive load, material is plastically deformed at the crack tip. Third step is when a tensile load is applied yet again, a new sawtooth has formed from the plastic deformation during compressive loading.*

fatigue can also be extracted from studies of striations, since the distance between striations depend on the applied load. In this work striations are mainly of interest since they may give information regarding crack propagation direction. Striations can be traced backwards to find the initiation point which is of main importance in this work.

2.4.2 Real metal

The slip-plane crack initiation described in Section 2.4.1 above is the ideal way for cracks to develop in a metal, but materials are not perfect and these imperfections become weak points where cracks can be initiated without formation of persistent slip planes. Examples of such weak points can be inclusions, pores or grain boundaries [11]. Crack initiation in fatigue can be viewed as a competition between all these different kinds of initiation mechanisms, the mechanisms that in the fewest amount of cycles creates a crack large enough for propagation will most likely "win" and dominate further crack growth. As the reader might imagine the type of initiation described in the section above is not very fast, numerous cycles are needed in order to create a large slip plane that may propagate as a crack. Thus if there are defects in the material large enough to initiate a cracks, an initiation by a slip plane mechanisms is not likely [11].

Consider an example of the inclusion of a hard (high E-modulus) and brittle particle in a soft (low E-modulus) metal matrix. When a load is applied the surrounding matrix will elastically stretch more than the inclusion, which will lead to that a stress concentration builds up around the particle. If the stresses becomes high enough the inclusion could rupture the matrix and a crack has been initiated. What process of crack initiation that occurs is if course not only dependent on material but heavily dependent on stress/strain range as well as temperature. The higher the stress/strain range, the smaller the minimum required size of weakness in the material. This is easily understood when considering the stress intensity range ΔK discussed in section 2.3.3.

For crack growth there is a threshold value ΔK_{th}, for a specific crack size there is thus a minimum stress range required in order for crack propagation to occur. If we consider a material containing a weakness of size a we will thus have zero initiation is the stress range applied is large enough. This is likely always the case in cast metals containing large casting defects [3] but also for fatigue at very high cyclic stresses [11]. At a large enough applied stress almost any weakness in the material is enough to immediately initiate a crack. Generally the distribution of life between propagation and initiation can be illustrated in a plot as in Figure 10.

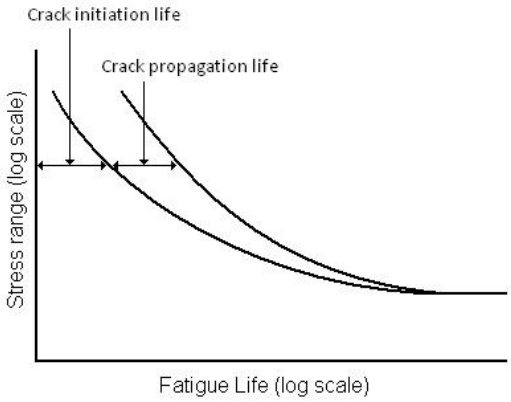

Figure 10: *A plot showing the typical distribution between initiation life and propagation life for different stress ranges. [1]*

The threshold value for crack propagation in combination with the fatigue limit $\Delta\sigma_{fl}$ may be used to approximate the maximum size of natural defects in a material using the Kitagawa-Takahashi diagram. This is done by calculating a from Equation 7 using $\Delta K = K_{th}$ and $\Delta\sigma = \Delta\sigma_{fl}$, for a surface defect a value of $f(g) = 0.7$ may be used. The reasoning behind this approximation is simple. Using the threshold value for crack propagation ΔK_{th} a stress level may be related to the maximum size of defects that would not cause propagation at this specific stress. At the fatigue limit the stress is low enough not to cause crack propagation even from the largest existing defects in the material, we know this since failure through fatigue does not occur. The defect size a calculated is thus the maximum size of natural defects in the material.

A Kitagawa-Takahashi diagram based on crack growth rate testing performed at Volvo Aero is illustrated in Figure 11. Test data used was performed at RT and 650°C with $R = 0$, the diagram shows maximum defect sizes of 74 and 270 μm respectively. Similar calculations has also been performed for $R = -1$ and $R = 0.5$ using both mean and minimum values of $\Delta\sigma_{fl}$. The results from all Kitagawa-Takahashi calculations are summarized in Table 1. Taking the mean of all calculated values the result is 0.19 and 0.46 mm for mean and minimum values of $\Delta\sigma_{fl}$ respectively.

The stage II propagation described in section 2.4.1 above is, much like the slip-plane initiation, also described in an idealistic way. Many factors affect the propagation of the crack, especially grain boundaries and defects such as inclusions or voids. It is natural for the crack to propagate along

Table 1: *A Table showing the results from Kitagawa-Takahashi diagrams where maximum natural defect size is approximated. Both mean and minimum values of fatigue limit has been used. Results are presented in mm.*

		$R=-1$	$R=0$	$R=0.5$
RT	$\Delta\sigma_{fl,mean}$	0.11	0.074	0.23
	$\Delta\sigma_{fl,min}$	0.24	0.12	0.39
400°C	$\Delta\sigma_{fl,mean}$	0.26	0.20	0.15
	$\Delta\sigma_{fl,min}$	0.74	0.45	0.30
550°C	$\Delta\sigma_{fl,mean}$	0.14	0.17	0.23
	$\Delta\sigma_{fl,min}$	0.58	0.37	0.60
600°C	$\Delta\sigma_{fl,mean}$	0.14	0.16	0.24
	$\Delta\sigma_{fl,min}$	0.21	0.37	0.63
650°C	$\Delta\sigma_{fl,mean}$	0.31	0.27	0.22
	$\Delta\sigma_{fl,min}$	0.67	0.57	0.72

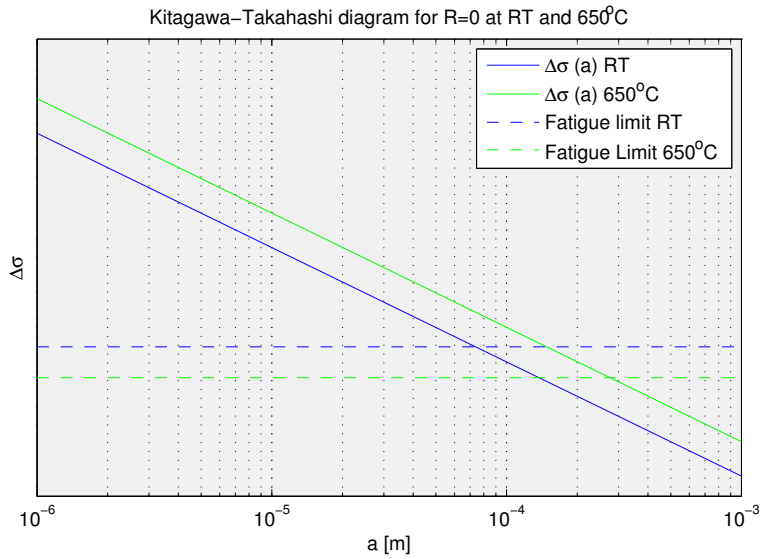

Figure 11: *A plot showing a Kitagawa-Takahashi diagram for Inconel-718 based on crack growth rate testing performed at Volvo Aero. At R=0 for RT and 650° C the diagram shows maximum defect sizes of 74 and 270 µm respectively.*

the weakest path and this makes the propagating fatigue crack an expert at finding different weaknesses in the material. Factors such as temperature have also been shown to affect how the crack propagates. In two articles by Andersson et al. the crack growth behavior in forged Inco-718 is investigated at high temperatures [14] and at room temperature [15]. It is found that crack propagation at room temperature is transgranular while crack propagation at high temperature ($687°C$) is intergranular. This is connected to weakening of grain boundaries with increased temperature.

2.5 Casting defects

Metal casting is the process of manufacturing components through pouring molten metal into a shaped mould, the metal is then cooled and the component takes solid form. The main advantage of casting is that it is the easiest way to manufacture large components with a complex geometry [16] but of course there are some drawbacks. It is a well known fact that mechanical properties, such as fatigue resistance, of cast components are considerably lower than properties of forged or wrought metal components.

At a first glance casting may seem to be an easy practice but if not done correctly the casting will contain numerous errors of different kind, casting defects, that will have a large impact on shape and mechanical properties. Numerous books have been written on this subject and many of the defects discussed are large and easily detected by visual or radiographic examination. This includes hot tears, mold shift or extensive pore formation. These kinds of defects are not of importance in this work since they are easily detected and castings containing such defects have not been included. Interesting defects should be such that a radiographic investigation cannot detect them. In this Section two kinds of such defects will be discussed, shrinkage defects and entrained bifilms.

2.5.1 Shrinkage defects

Shrinkage defects is a wide term used for any kind of defect created due to the shrinkage of molten metal in the transition from liquid to solid. In size they may vary from macroscopic voids in the material, easily detected by the human eye, down to 10th of a micrometer features that will pass through a radiographic investigation without detection.

To prevent formation of shrinkage defects molten metal is fed to the casting throughout solidification of a component. Defects arise when new liquid metal is somehow prevented to flow by early solidification in flow critical

areas. If the total inflow of feed metal is hindered a large macroscopic void will be created but inflow can also be hindered in smaller regions of the casting. The latter case is the one of interest in this work and is often called shrinkage porosity. If small enough a pore may pass through a radiographic investigation and initiate a fatigue crack, if a cluster of pores gather it may have devastating implications on fatigue life.

2.5.2 Bifilms

Despite casting being an ancient practice some interesting advances have been realized the past decades through the contributions of John Campbell and others. In numerous articles and books Campbell has presented his theories behind the formation of casting defects [3][17][18]. According to Campbell one of the most common casting defect is due to surface oxides that have been entrained, or folded into, the molten metal.

Metals are generally reactive elements that easily form compounds. Even in solid form many pure metals are susceptible to reactions with the environment, oxidation is one such common reaction. Molten metal is of course even more reactive and will immediately form oxides when in contact with air. These oxides will form on the surface of the melt and protect against further oxidation but when the metal flows turbulently, for example when molten metal is poured into the mould, these oxides will fold and become entrained into the molten metal, see Figure 12 [17]. The metal oxides are solid ceramic compounds that do not mix with the molten metal, thus when entrained they may form a pre-cracked region where cracks may initiate easily. Molten Aluminum, Titanium and Chromium are elements known to easily form oxides when in contact with air, Inconel-718, the nickel-base alloy investigated in this study, contains all of these elements.

The impact of pouring was first investigated in an article by Green and Campbell in 1994 [19]. In experiments an aluminum alloy was produced under identical conditions with one exception; the metal was poured into the mould differently. Some moulds were filled very cautiously and some very turbulently. The article showed that mechanical properties of the components varied depending on the degree of turbulence while pouring. The authors tied the difference in properties to the amount of bifilm content entrained into the cast components due to turbulence.

In continued investigations the initiation sites of fatigue samples of an aluminum-silicon alloy were studied [20][21]. The authors concluded that in 98% of all investigated samples the cause of initiation were entrained bifilms. The remaining 2% were initiated through a slip-plane mechanisms and had a

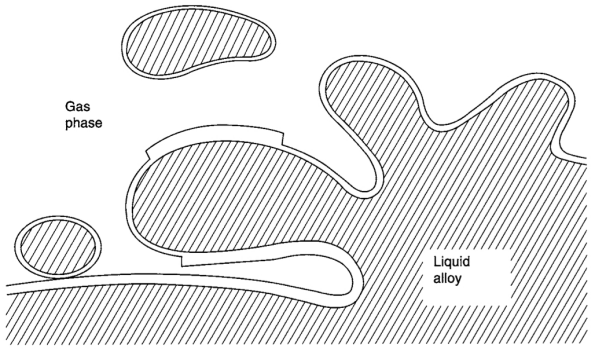

Figure 12: *A schematic picture showing how oxides formed on the surface of molten metal could easily become entrained during turbulent pouring. [17]*

fatigue life of up to 100 times higher than the defect samples.

The aerospace industry has of course noted the potential damage oxide formation has in the form of dross or bifilm entrainment. In order to reduce these effects all nickel-base superalloys containing oxide reactive elements are cast in vacuum. By the use of induction heating the metal is melt within a vacuum container and later poured into the mould that is also kept inside the same container. Although it does reduce oxide formation this method does not completely remove the issues according to some scientists. Campbell regards the industrial vacuum used as mere "dilute air" [17] that is not sufficient to prevent the formation of oxides.

In a study performed at Volvo Aero a new casting method was evaluated. Instead of vacuum a protective environment of Argon was used, the hope was that this could work equally well without having to bother with vacuum pumping. Selected cross sections of an Inconel-718 sample cast using the Argon method was polished and investigated in a microscope and SEM. The polished cross sections showed signs of entrained bifilms, as seen in Figure 13. Energy-Dispersive X-ray spectroscopy (EDX) was also used to study the elemental composition of the oxides formed. The analysis showed them to be rich in Al and Ti, heightened values of Nb was also measured.

2.6 Material

The fatigue samples investigated in this report are produced in the same manner as most cast components of oxide forming alloys used in the aerospace industry, through investment casting in vacuum. The mould is in the shape of a large ring, thus the samples are not shape cast. From this ring mate-

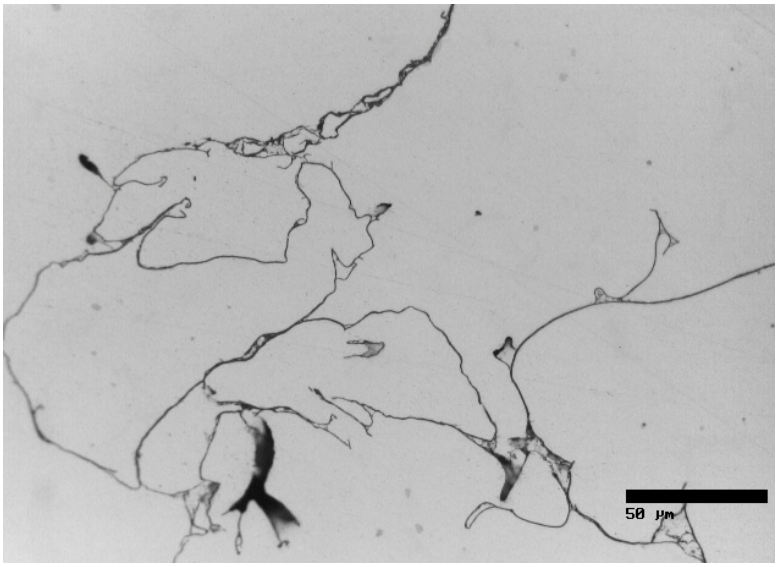

Figure 13: *A picture over a polished cross-section of an Inconel-718 casting taken at 500x in an optical microscope. The casting was produced in a protective environment of Argon instead of the otherwise commonly used vacuum. The image clearly shows that entrained bifilms are present in the material.*

rial is cut and turned into the shape of smooth cylinders. Shape casting is avoided since it would not simulate the critical areas of a Inconel-718 component. These are often large casings and critical areas are for example holes drilled during the post casting processing. If the samples had been shape cast the grain size at the surface would not represent the grain size at the surface of a drill hole, this would make testing inaccurate. Prior to testing the cast rings are heat treated and exposed to Hot-Isostatic Pressing (HIP).

The fatigue samples tested in this report comes from three identically produced casting batches. The majority of samples ($\sim$ 80 %) comes from one batch and the remaining 20 % is evenly chosen from the other two batches. Results of fatigue testing have been reported to differ from batches manufactured under nominally identical production conditions [22]. In this report small differences between batches will only make the results more interesting however.

The microstructure of tested samples, investigated by polishing and etching a cross section taken from a fatigue sample is depicted in Figure 14. The microstructure is clearly of dendritic nature, both primary and secondary dendrites are visible in this image. Weaknesses, such as pores or entrained bifilms will gather in regions between dendrites due to dendrite pushing during solidification of the alloy. Unwanted phases that may be formed

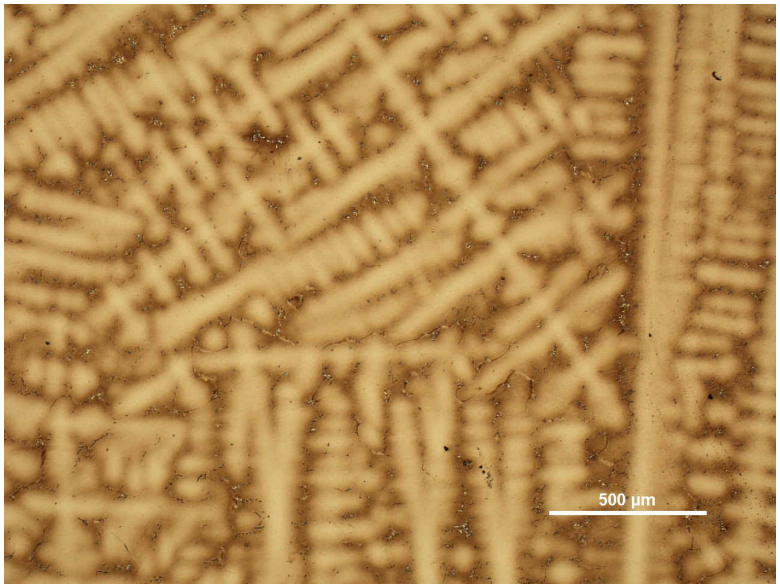

Figure 14: *A picture over a polished and etched cross section through a fatigue sample, taken in an optical microscope at 50X. The picture clearly shows that the microstructure of cast Inconel-718 is of dendritic nature.*

through strong material segregation, such as laves phase, are also found in interdendritic regions.

The notched samples that have been investigated have been manufactured from smooth cylinders, similar to the LCF samples investigated in this report. The cylindrical samples were notched such that $K_t = 2.0$.

3 Numerical calculations

In order to complement the fractographic investigations numerical calculations have been performed, the purpose of the numerical calculations is to give an approximate value of crack propagation life. The total fatigue life of each sample is known and thus an approximate value of initiation life can be acquired. Initiation life is of importance to determine what kind of initiation mechanism that is active in the fatigue samples. If total life is found to be governed by propagation only it is likely that cracks originated from a very weak or even pre-cracked region, for example a casting defect.

As previously mentioned an initial crack size a_i is required in order to calculate propagation life using fracture mechanics. This a_i has been measured through fractographic investigations for all samples where an initiation point could be found. Numerical calculations have been made using NASGRO, a fatigue crack propagation analysis tool developed by SouthWest Research Institute for NASA. Input parameters are R-ratio, stress range, initial crack size, crack type and most importantly material data. The material data used for the calculations were acquired from testing of Inconel-718 performed at Volvo Aero, how this data is acquired is explained in section 2.3.3.

In order to accurately compute propagation life for different crack types NASGRO contains a range of different standard choices of crack type and component structure. Both surface and subsurface initiations have been found in this work, and two different cases have been used to model each type of initiation. Surface initiations were approximated by a near half-circular crack shape, the structure chosen was a solid cylinder, in order to simulate a fatigue sample, as shown in Figure 15. In this approximation c and a are related through

$$a = r(1 + \tan\theta - \sec\theta),\ \theta = \frac{c}{r} \tag{10}$$

and either one of the parameters are used as input. For the subsurface initiations an embedded elliptic model as in Figure 16 have been used. Here a and c are separate parameters that are input along with distance from surface B_t and B_w. In this model the structure is not a cylinder like the fatigue samples modelled, however the small difference in structure should have a modest effect on the total propagation life calculated since the majority of fatigue life is expended when the crack is small.

NASGRO calculates propagation life by step-wise integration of eq 9 from a_i until an ending condition has been met. Different choices of ending condition is possible, in this work the ending condition was met when global stress exceeded flow stress. Flow stress is assumed to be the average of yield strength and ultimate strength, properties measured during testing.

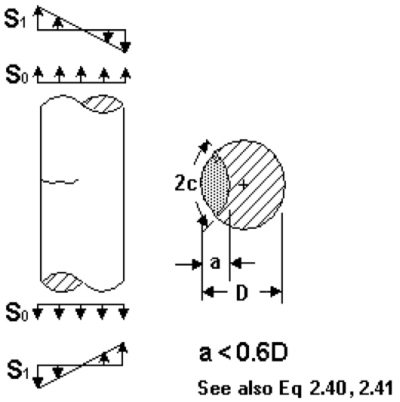

(a) Surface crack approximation model

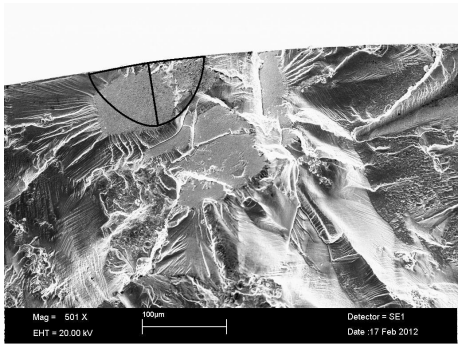

(b) Surface crack approximation applied

Figure 15: *Two images showing how the initial size of surface cracks has been approximated* ***a)*** *Model used by NASGRO, a thumbnail crack of depth a in solid cylinder of diameter D [10].* ***b)*** *Picture showing the crack size approximation applied to a real surface initiation.*

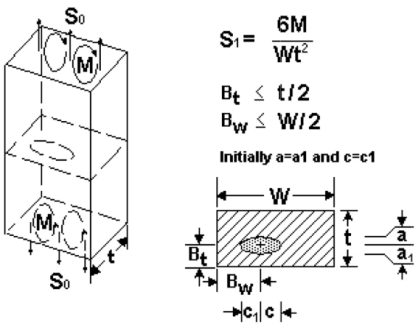

(a) Subsurface crack approximation model

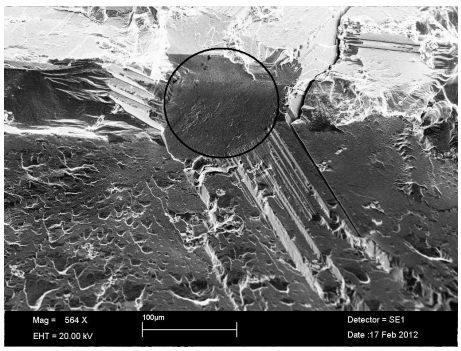

(b) Subsurface crack approximation applied

Figure 16: *Two images showing how the initial size of subsurface cracks has been approximated* ***a)*** *Model used by NASGRO, an embedded crack of elliptic shape in a solid rectangular plate [10].* ***b)*** *Picture showing the crack size approximation applied to a real subsurface initiation.*

4 Results

In total 62 different smooth samples, both HCF and LCF, as well as 11 notched samples have been investigated and documented using SEM. LCF samples were solely $R = 0$ samples, 25 of them were tested at 650°C and 18 at Room temperature (RT). Out of the 19 HCF samples 10 were tested at 650°C and 9 at RT. The notched samples were tested under R=0 and 550°C condition.

The fractographic investigation was aimed at measuring the size of initiation point as well as to determine the cause of initiation if possible. The measured initiation sizes were then used as input in crack propagation calculations.

4.1 Fractographic investigation of smooth samples

4.1.1 Room temperature samples

At RT and R=0 all initiations were found at the surface of the sample.Two typical examples of surface initiations at RT is shown in Figure 17. In Figure 17(a) we see a facet initiation of $\sim 100\,\mu m$ size. It has a well defined boundary, the darker areas are likely oxidations. In Figure 17(b) an initiation difficult to determine is depicted. It is difficult due to the crack propagation mode that leaves a cleavage-like fracture surface where initiation is difficult to distinguish from propagation.

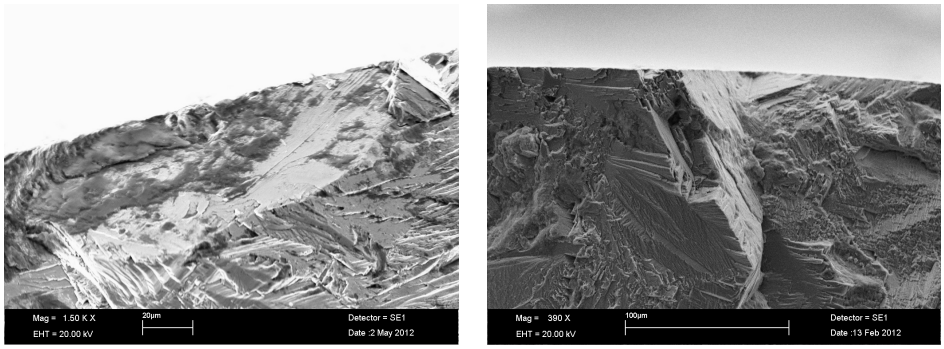

(a) RT surface initiation 1 (b) RT surface initiation 2

Figure 17: *Two images showing two examples of surface initiations in samples tested at room temperature and R=0 condition.* ***a)*** *A quite large initiation facet that was easily identified.* ***b)*** *An overview of a surface initiation. In this case it is difficult to determine a precise initiation site, this much due to the cleavage-like and coarse propagation of the fatigue crack.*

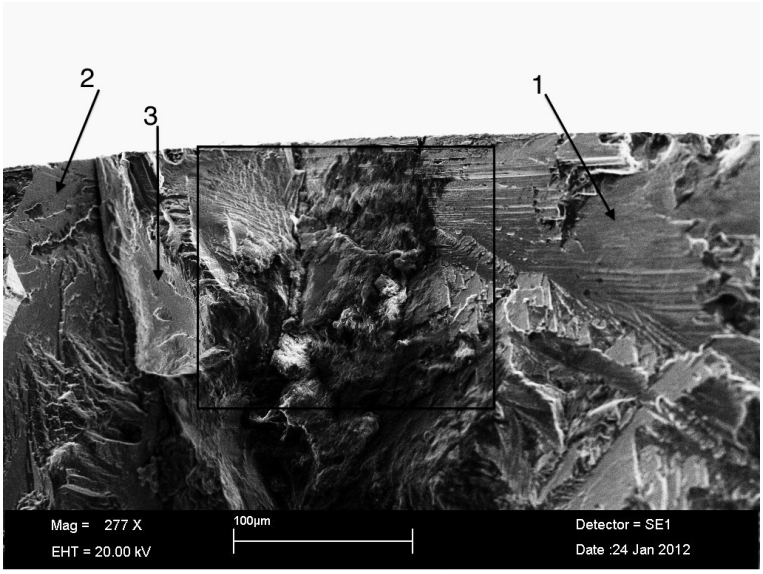

Figure 18: *A picture showing an initiation where it has been difficult to determine the exact initiation. The rectangle indicates the general initiation area. Arrows point at areas where crack propagation has been cleavage-like and at a high angle toward the fracture plane.*

A good example of this cleavage-like crack propagation is seen in Figure 18. In this fractograph the general initiation area is marked in the rectangle, determination of the exact initiation is however difficult. The darker areas within this rectangle are likely oxides. Arrows marked 1,2 & 3 point at areas where crack propagation is along a high angle towards the fracture plane.

4.1.2 High temperature samples

At 650°C and $R = 0$ 75 % of the 25 investigated samples were found to have been initiated at the surface of the samples, the initiation feature had a facet like appearance. In close to all cases the surface initiations had a very similar appearance which implies that the initiation mechanism is also similar. The remaining 25% were found to have been initiated at a sub-surface location. For sub-surface initiations the appearance could differ, the initiation was tied to either unwanted material phases or a flat facet-like feature quite similar to the surface initiations.

Two typical surface initiations at 650°C can be seen in Figure 19. In Figure 19(a) we can clearly see the initiation facet in the center, the facet in this image is around 80x50 μm in size. The facet appears bright due to that it is at an angle towards the secondary electron detector. From this central facet

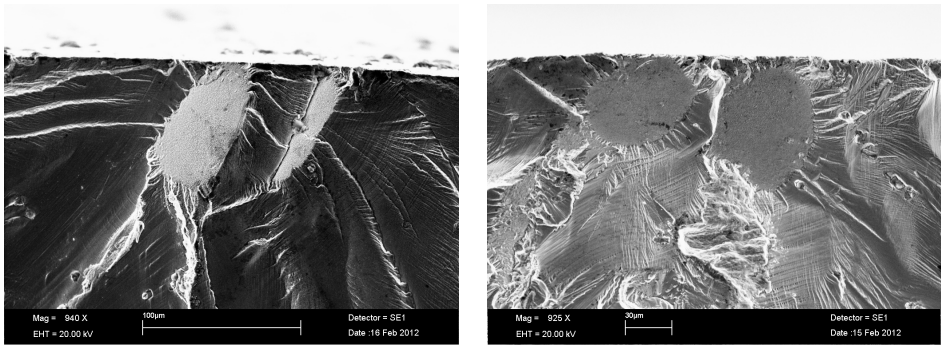

(a) 650°C surface initiation 1 (b) 650°C surface initiation 2

Figure 19: *Two images showing two examples of surface initiations in samples tested at high temperature and R=0 condition.* ***a)*** *Two facet surfaces that initiated the crack. The larger facet surface seems to be the true initiation, the smaller facet to the right is a pre-cracked region that the fatigue crack has encountered during growth. Surrounding matrix is non-defect material judging from the riverine features.* ***b)*** *A case very similar to the previously described, judging by the crack propagation signs the left facet is the true initiation point.*

we can distinguish the fatigue crack growth in all directions from the riverine features. These are also signs of proper metallic binding in this area, i.e non-defect material. To the right of the larger facet we see a secondary facet that the crack has encountered during growth, the narrow line of shadow seen at the left edge of the secondary facet seems to indicate that this facet continues further into the material . Figure 19(b) is of the same nature, the leftmost facet is the initiation and the rightmost facet has been encountered during crack growth. An additional surface initiation at high temperature can be seen in Figure 15(b).

Figure 20 show two typical sub-surface initiations found at high temperature. Figure 20(a) show the most common sub-surface initiation. The appearance of this kind of initiation is very much similar to the surface initiations found at high temperature, a round facet of $\sim$ 100 μm size. Early crack propagation however differs substantially from the surface initiation case. At high temperatures early crack propagation is typical stage II fatigue from surface initiations, from sub-surface initiations the early crack propagation is however more similar to stage I fatigue. Early crack propagation leaves a very smooth facet-like surface, often at a large angle towards the fracture plane which is the case here.

The facet appearance of early crack propagation in internal initiation is proof of transgranular (through grains) crack propagation. The crack grows along a crystallographic plane which leaves a smooth fracture surface. The size of these facets may differ considerably between different samples, the termina-

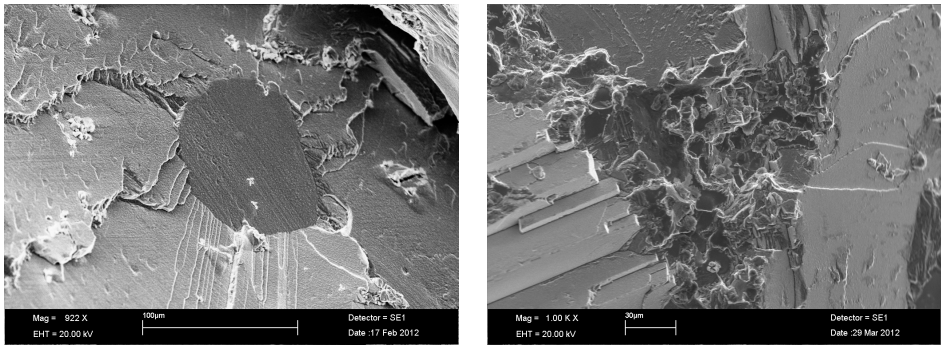

(a) 650°C sub-surface initiation 1 (b) 650°C sub-surface initiation 2

Figure 20: *Two images showing two examples of sub-surface initiations in samples tested at high temperature.* ***a)*** *A sub-surface initiation quite similar to the surface initiations seen at high temperature. The crack propagation forms a facet-like fracture surface that grows at a large angle towards the fracture plane.* ***b)*** *A rare sub-surface initiation. Early crack propagation forms facet surfaces in all directions as was found in the other sub-surface initiations as well.*

tion of this type of crack propagation is likely connected to the encounter of a grain boundary or sample surface.

Figure 20(b) show a less common sub-surface initiation type. The fractograph shows signs of brittle fracture in the initiation and early crack propagation leaving a facet surface. As above this facet surface is formed through crack growth along a crystallographic plane in one grain, this is especially apparent from the crack propagation to the left of the initiation where shelf-like structures are formed. The initiation does not have the appearance of a pre-cracked region, the cause of initiation may be related to the elemental composition in the area. If impurities or unwanted weak material phases are present they could compose a weakness that is a possible crack initiation site. An additional sub-surface initiation at high temperature can be seen in Figure 16(b). The initiation feature is similar to sub-surface initiation 1 (Figure 20(a)) discussed above and the initial crack propagation is almost identical to above mentioned cases.

Studies of fracture surfaces has not only focused on finding initiations, other remarkable features have also been noted. One such feature often seen is depicted in Figure 21. The picture shows a sub-surface feature within the fatigue area. The area appears perfectly smooth in the darker areas, i.e there are no fine striations. In an optical microscope the area that is dark in the image appears shiny and reflects lights, almost as a mirror.

The absence of striations and the fact that the feature is smooth even though it is not cut straight as a facet is proof that the feature is related to some

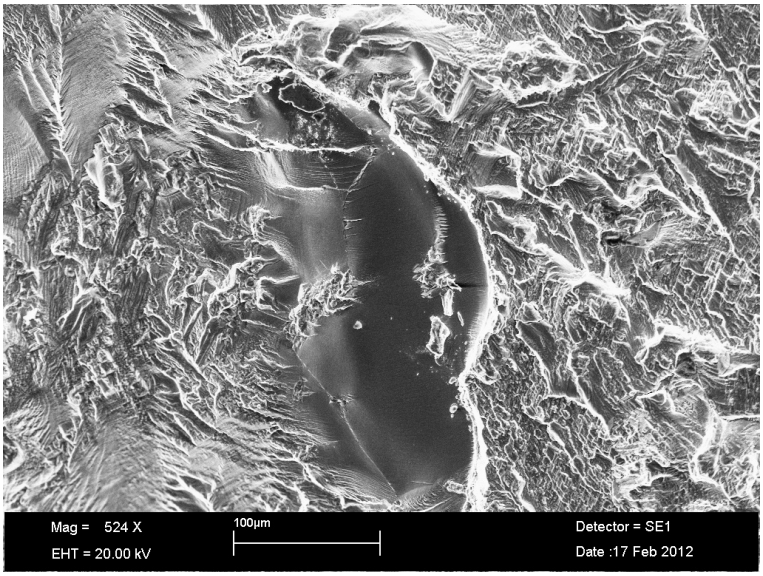

Figure 21: *An image showing a striking feature found in the fatigue area of a fracture surface of a high temperature LCF sample. The feature is very smooth, no fine striations may be found at higher magnification.*

kind of weakness in the structure. Had the region been pre-cracked it would likely have initiated a crack. Judging from crack propagation signs this region seems to have been found by a propagating crack rather than to have initiated a crack. The feature is in size comparable to the dendrites seen in Figure 14. To be noted is that this kind of feature is often appearing in high temperature samples, but never for RT samples.

4.1.3 Initiation size measurements

The measured sizes of surface and sub-surface initiations are plotted against stress range in Figure 22. Several initiations in a single sample have been quite uncommon, but in the cases where several initiation have been found the largest initiation point was chosen. Initiation areas at low stresses is considered to be accurately measured but initiations have been very difficult to measure accurately in non-notched samples at high stress ranges, the uncertainty is therefore quite high in this stress range. The stress rages for the notched samples is given in stress at notch and not nominal stress.

Approximate crack sizes according to

$$a_i = \sqrt{A} \tag{11}$$

is in the range of 40-170 μm. This in quite good accordance with values

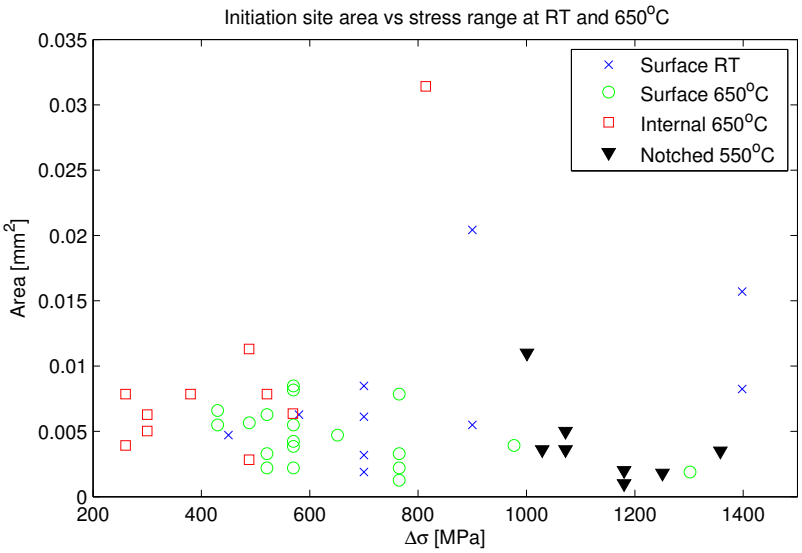

Figure 22: *A plot showing the measured area of surface and sub-surface initiation points for samples at RT and 650° C plotted against stress range. The measured initiation area does not depend on stress range. Included samples are both HCF and LCF, since LCF tests are strain controlled their corresponding stress range was calculated using Hooke's law.*

of maximum defect size calculated using Kitagawa-Takahashi diagram described in Section 2.4.2. For $R = 0$ condition at RT and 650°C the approximated maximum defect size is calculated to be 74 and 270 μm respectively.

The main result from the plot is that area of initiations is independent on stress range, however the site of initiation is not independent on stress range. For a low stress range the typical initiation is internal and the probability of an internal initiation decreases as stress range is increased. The initiations measured in notched samples are smaller on average compared to initiations measured in smooth samples.

The outlier at $\sim 820\ MPa$ is an internal initiation of type depicted in Figure 20(b). The larger area measured could be connected to a deviating initiation mechanism.

Figure 23 show a tweaked Stress-Life plot, where a gray scale has been included to simultaneously show the crack size. The filling color of each data point corresponds to the crack size in mm according to Equation 11. For surface initiations at RT there is hardly any correlation between large initiation and short life, this is likely connected to the difficulties of measuring the initiation site accurately. For high temperature surface initiation there is a

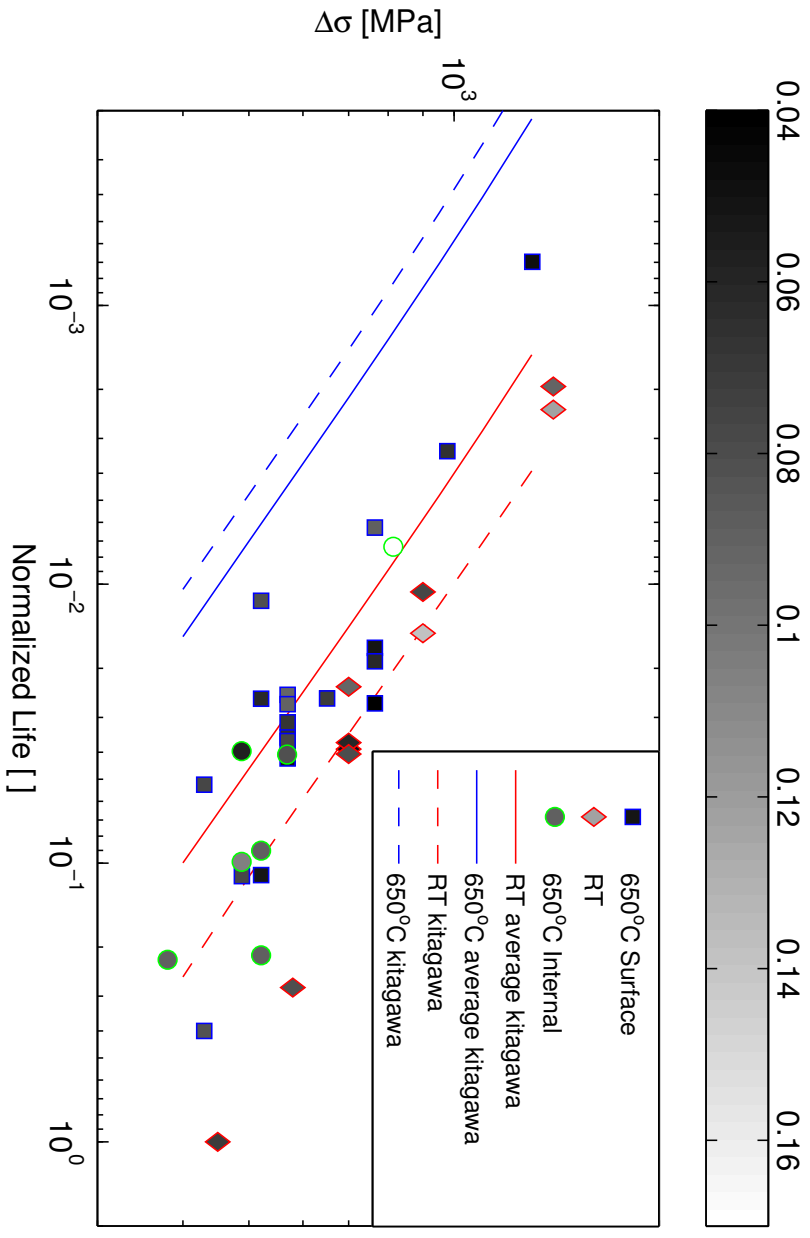

Figure 23: *A plot showing a stress-life plot of investigated samples, also displaying size of measured initiations through gray scale filling of symbols. The white end of the scale corresponds to the maximum initiation found and the black end to the minimum initiation. The scale is crack size (mm) calculated through* $a = \sqrt{A}$*. High temperature surface initiations show a good correlation between life and size of initiation, the agreement is worse for high temperature internally initiated samples and room temperature samples. Life has been normalized in order to maintain confidentiality. Included samples are both HCF and LCF, since LCF tests are strain controlled their corresponding stress range was calculated using Hooke's law. Plot also incudes results from numerical calculations where initiation sizes approximated with Kitagawa-Takahashi diagrams were used as start cracks.*

very good agreement between short life and large initiation. The agreement for high temperature internal initiation is not so good either. This though is expected since there are other variables that decides life in sub-surface initiated samples, mainly distance from initiation to the surface. A large distance between initiation and surface leads to a longer life.

Figure 23 also show four curves where life has been calculated using NASGRO for some different stress ranges at $R = 0$. This is further commented in Section 4.3.

4.2 EDX analysis

Energy-Dispersive X-Ray spectroscopy (EDX) analysis has been performed on selected surfaces, the main purpose was to investigate the elemental distribution and amount of oxides present near initiation areas.

Figure 24 show the results from a EDX analysis of the surface initiation in Figure 17(a). To the left in Figure 24(a) crack growth is along a high angle towards the fracture plane, where shearing forces are high. On this surface there is an eye-catching feature with a dark and coarse appearance, this feature is rich in oxides as shown by Figure 24(b). Part of the facet, the darker area, is covered in a thick oxide (Figure 24(c)), while other areas on the initiation facet show no signs of oxide coverage (Figure 24(d)). This result is the typical case for RT initiations.

The oxides covering the facet and other areas could have been introduced from the environment post fatigue testing but there are no indications of elements alien to Inconel-718, which makes this explanation void. The oxides are likely not formed from normal oxidation of the fracture surface either, an equally thick layer of oxides covering the entire fracture surface would then have been observed. The oxides could also have been caused already in the melt during casting and entrained within the material, forming a bifilm defect as previously discussed in Section 2.5.2. However the EDX analysis does not show increased rates of elements prone to form oxides in the melt, such as aluminum and titanium, as would have been expected.

A probable explanation is that the dark and coarse area near the initiation is the result of fretting between the two fracture surfaces. Fretting between surfaces produce a lot of debris in the form of small metal particles. These particles are easily oxidized post fatigue due to their large surface area and they could easily spread in the vicinity of the fretting during fatigue testing. This would explain the existence of oxide on the initiation facet.

Figure 25 show another RT initiation. The results are similar to the above

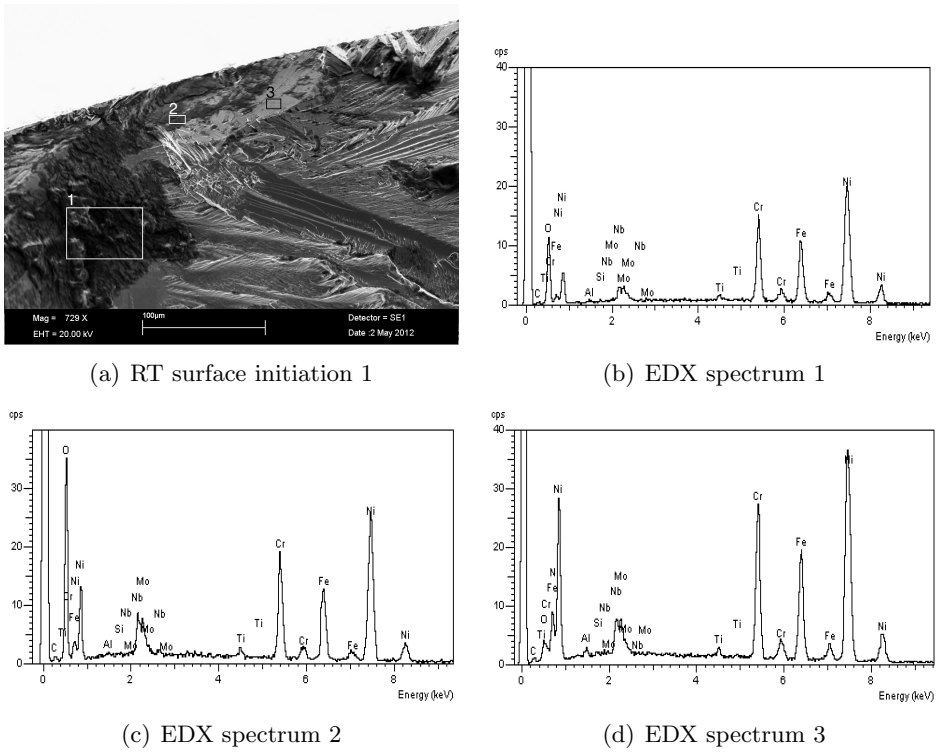

(a) RT surface initiation 1

(b) EDX spectrum 1

(c) EDX spectrum 2

(d) EDX spectrum 3

Figure 24: *EDX investigation of a RT surface initiation.* ***a)*** *Fractograph over the initiation, marked areas show where EDX spectra has been taken* ***b)*** *EDX spectrum of the leftmost area, the overall count per second (cps) of the detector is low here due to the roughness and inclination of the surface. Looking at the ratio between cps of Ni and O we can see that the area is heavily oxidized.* ***c)*** *EDX spectrum of the middle area, the area is covered with oxides.* ***d)*** *EDX spectrum of the rightmost area, close to no oxides are present here.*

discussed case, an initiation facet is visible with some amount of oxides present in the near vicinity. There is no fretting surface found in the vicinity of the oxides but as above the oxides are not rich in Al or Ti, it is therefore not likely that the oxides were formed during casting and entrained in the material.

Figure 26 show the results from an EDX analysis of a surface initiation from a high temperature sample. The initiation of this sample has been previously discussed in Section 4.1. The first spectrum show signs of oxides, for a high temperature sample this is expected since a layer of oxides covering the whole fatigue surface is produced during testing. The second spectrum taken on the larger surface facet show signs of a considerably higher oxide content compared to the average fatigue surface. The last spectrum is taken of a small deviating particle at the smaller initiation facet. The particle seemingly consists almost entirely of Al and Si oxides. It is unclear whether

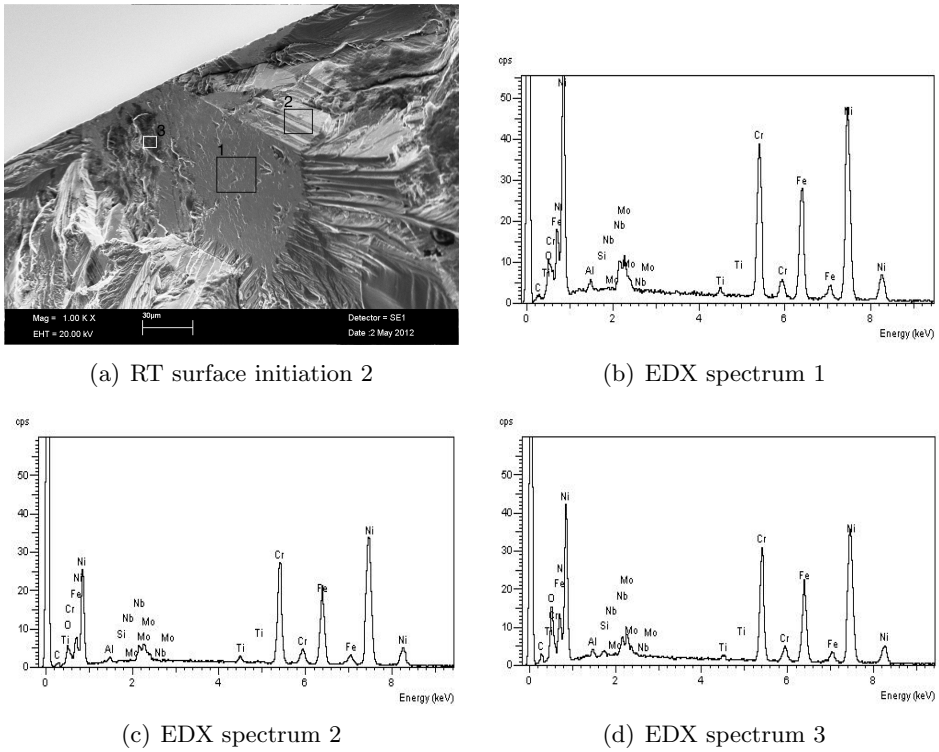

(a) RT surface initiation 2

(b) EDX spectrum 1

(c) EDX spectrum 2

(d) EDX spectrum 3

Figure 25: *EDX investigation of a RT surface initiation.* ***a)*** *Fractograph over the initiation, marked areas show where EDX spectra has been taken* ***b)*** *EDX spectrum of the central area numbered 1, the facet show close to no signs of oxides.* ***c)*** *Area numbered 2 just outside the initiation facet, close to no oxides are present here. Overall the spectrum is similar to area 1 but the total cps is lower due to surface alignment.* ***d)*** *The darker area numbered 3 closer to the surface, this area is seemingly rich in oxides.*

this particle has been introduced post fatigue or if it was entrained in the melt during casting.

Figure 27 show the results from an EDX analysis of the sub-surface initiation depicted in Figure 16(b). The initiation facet and surrounding propagation facets are covered in a thick oxide layer. Compared to the average oxide coverage of the fatigue surface the facet surfaces are more heavily oxidized.

Figure 28 show a fractograph and EDX analysis of the initiation depicted in Figure 20(b). The initiation show signs of brittle failure and subsequent facet crack growth along crystallographic planes. EDX analysis show the surrounding facet surfaces to be rich in oxides, which is expected for samples tested at high temperature. The elemental composition of the facet surfaces otherwise represent that of Inconel-718. The EDX spectra taken within the initiation show that the elemental composition varies greatly, specifically the

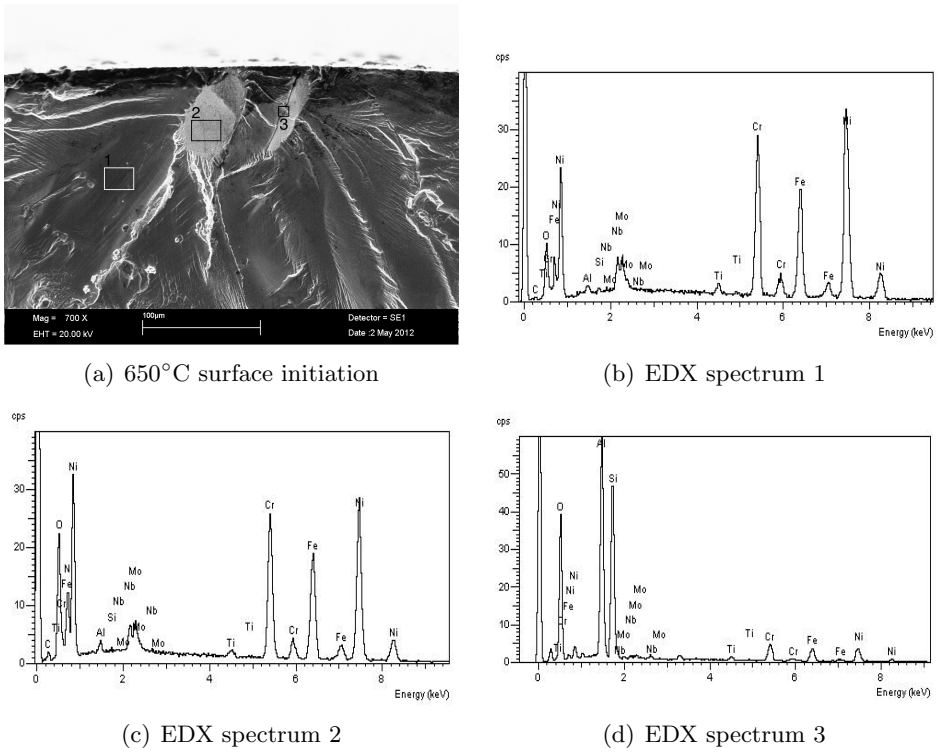

(a) 650°C surface initiation

(b) EDX spectrum 1

(c) EDX spectrum 2

(d) EDX spectrum 3

Figure 26: *EDX investigation of a high temperature surface initiation.* ***a)*** *Fractograph over the initiation, marked areas show where EDX spectra has been taken* ***b)*** *EDX spectrum of the leftmost area, oxides are present in this area but that is expected. At 650° C the whole fatigue surface is covered in oxides during testing.* ***c)*** *EDX spectrum of the middle area, the surface facet is covered in oxides to a larger extent than EDX spectrum 1. The smaller facet to the right is likewise covered in oxides.* ***d)*** *EDX spectrum of the rightmost area, a deviating particle seemingly situated on the surface of the smaller facet. The particle seems to consist of almost entirely Al and Si oxides.*

rate of Nb and Mo. As was mentioned in Section 2.1 the amount of Nb is one tenth of the amount of Ni, but as seen in Figure 28(f) the cps for Nb is even higher than that of Ni in some areas within the initiation.

4.3 Crack propagation calculations

A crack propagation calculation was performed for each sample where an initiation site could be determined, the size of the initiation site a_i was measured from fractographs. Propagation life was calculated using NASGRO assuming an initial crack size a_i, the assumption is thus that the material is pre-cracked and the size of the initial crack corresponds to the size of

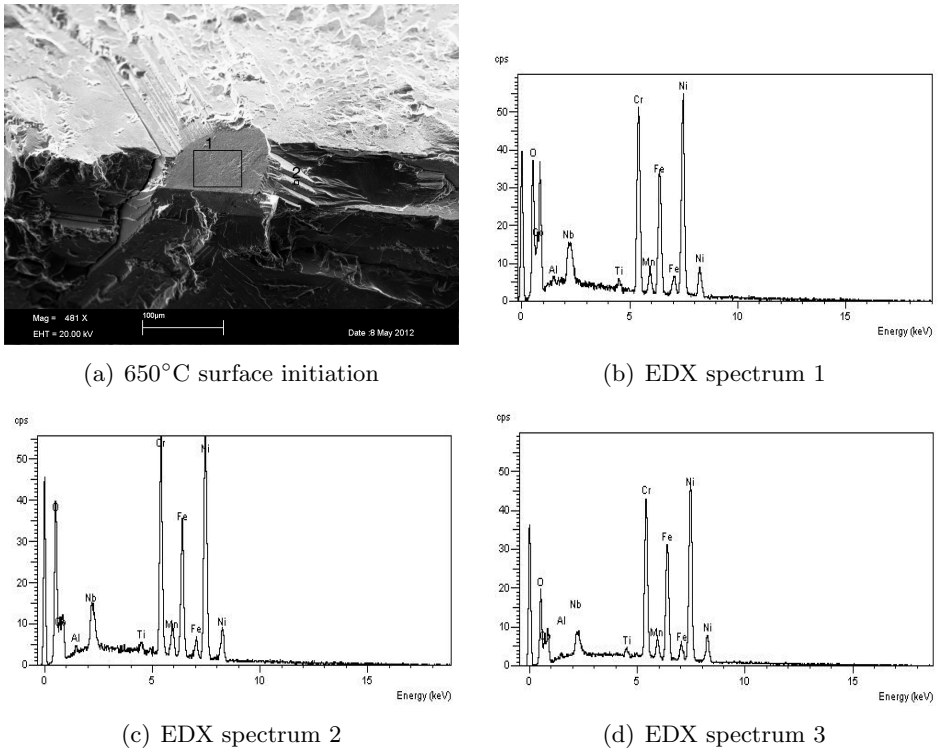

(a) 650°C surface initiation

(b) EDX spectrum 1

(c) EDX spectrum 2

(d) EDX spectrum 3

Figure 27: *EDX investigation of a high temperature surface initiation.* ***a)*** *Fractograph over the initiation, marked areas show where EDX spectra has been taken* ***b)*** *Spectra from the initiation facet, a high amount of oxides are present.* ***c)*** *Spectra from the shelf-like facet to the right of the initiation facet, a high amount of oxides are present.* ***d)*** *Spectra taken over a large fatigue area of stage II propagation. Oxides are present here as well but at a lower rate compared to the facet like structures.*

the initiation site. The results are presented as plots of the ratio between actual life of a HCF or LCF sample and calculated life for each corresponding sample vs stress range. Crack propagation calculations have also been performed using a_i calculated from Kitagawa-Takahashi diagrams.

4.3.1 Samples at room temperature

The main result from crack propagation calculations for room temperature samples can be seen in Figure 29. The plot shows that we have a good agreement between calculated and actual life with some outliers at $\Delta\sigma \approx 900$ & 450 MPa. The outlier at 450 MPa is likely related to a long initiation stage that is not considered by the numerical calculation. At this stress range the fatigue limit is close and many cycles might be required before the

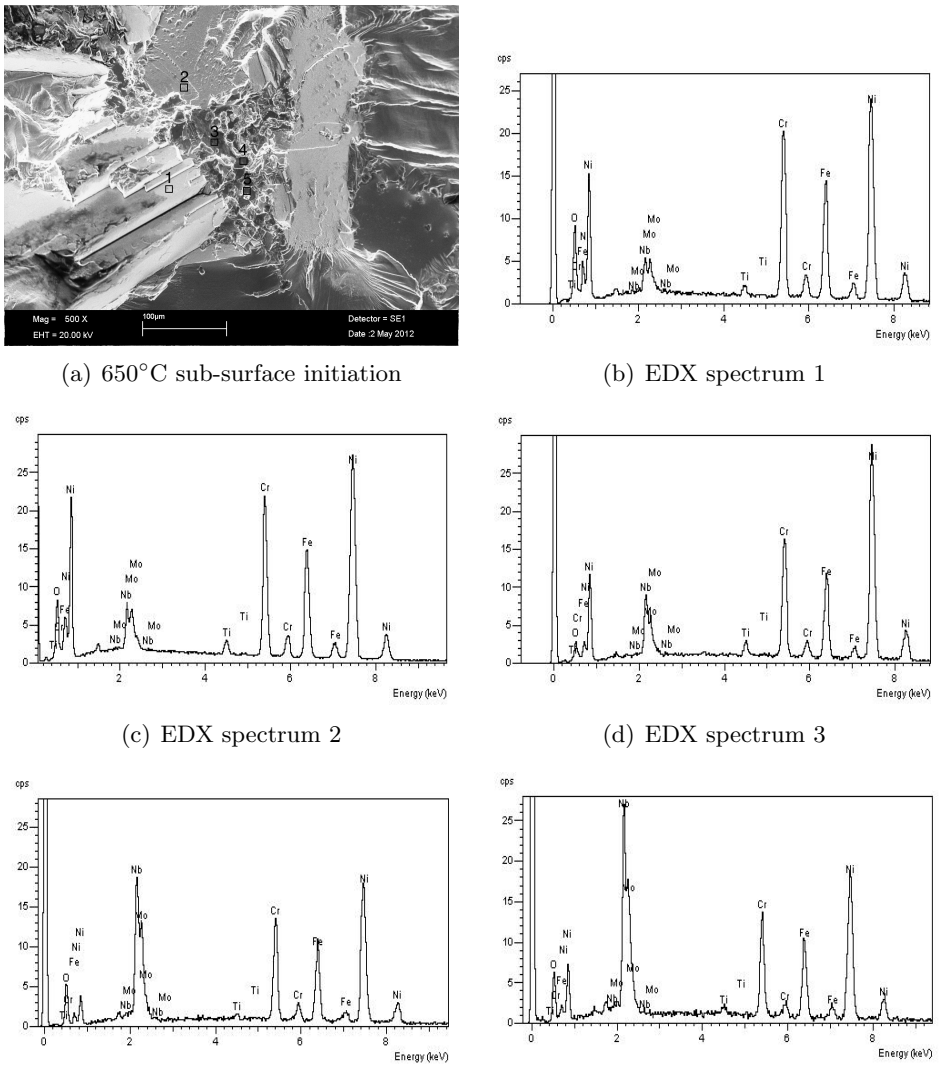

(a) 650°C sub-surface initiation

(b) EDX spectrum 1

(c) EDX spectrum 2

(d) EDX spectrum 3

(e) EDX spectrum 4

(f) EDX spectrum 5

Figure 28: *EDX investigation of the high temperature sub-surface initiation depicted in Figure 20(b).* ***a)*** *Fractograph over the initiation, marked areas show where EDX spectra has been taken.* ***b)c)*** *EDX spectra over the facet areas outside the initiation, oxides are present which is also expected for a high temperature sample.* ***d)e)f)*** *EDX spectra of areas in the initiation. The elemental composition varies greatly over the area, specifically the content of Nb and Mo which is very high in spectrum 4 and 5.*

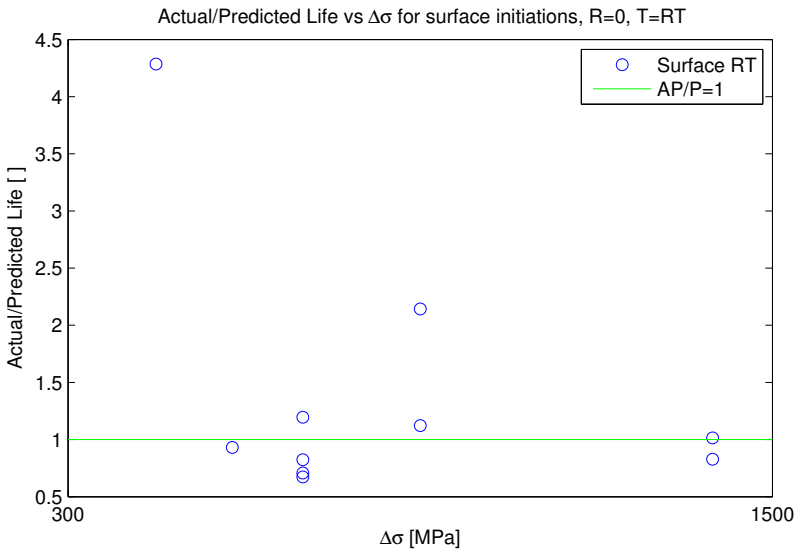

Figure 29: *A Plot showing actual life divided by propagation life vs cyclic stress range for samples tested at room temperature.*

weakness is considered a propagating crack.

4.3.2 Samples at 650°C

The main result from crack propagation calculations for samples at 650°C can be seen in Figure 30. The agreement between calculated propagation life and actual life is good but far from excellent. The mean of the data is seemingly distributed around $A/P \approx 3$, that is on average we predict a life that is one third of the actual life. The agreement between calculated and real values is comparable for both surface and sub-surface initiations.

4.3.3 Calculations using a_i from Kitagawa approximations

These results are presented in Figure 23 as lines. The starting crack size a_i was taken as the calculated values of maximum defect in the material using Kitagawa-Takahashi diagrams, see Table 1. Blue lines were calculated using crack propagation data at 650°C and red lines crack propagation data at RT. For each temperature two different sizes of a_i was chosen, average kitagawa and the kitagawa size corresponding to each temperature. Average kitagawa was taken as the average of all mean kitagawa-sizes at different temperatures and R-values, which is 0.19 mm.

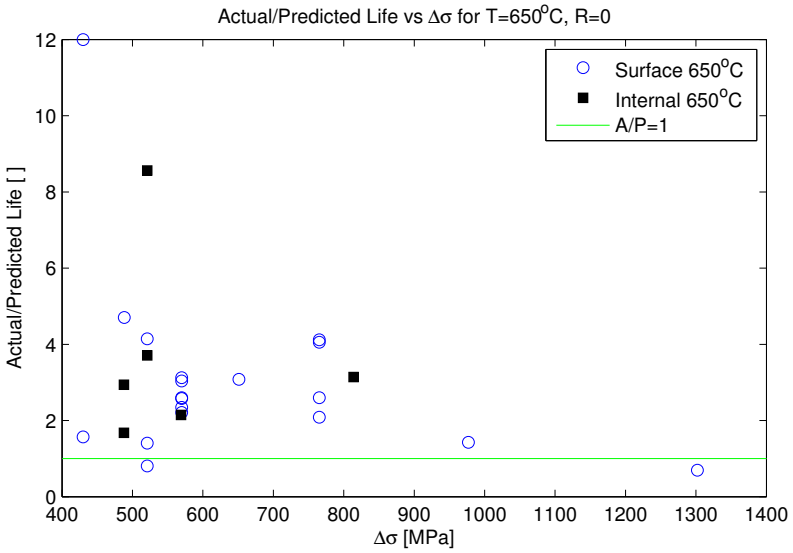

Figure 30: *A Plot showing actual life divided by propagation life vs cyclic stress range for samples tested at 650° C and initiated at the surface.*

The results show mainly the same results as has already been presented. Approximating life using RT crack propagation data gives a good agreement between actual life of RT samples and calculated life. For high temperature samples the calculated life is conservative.

4.4 Notched samples

Results from fractographic investigations of notched samples show that small facets at the surface are main initiators, much similar to the surface initiators at high temperature for polished samples. Two typical initiation points from a notched sample exposed to a high load is depicted in Figure 31. The specific sample was initiated at ≥ 5 points along the notch, all initiations shared the same appearance. As expected the largest initiation, seen in Figure 31(a), was found in the primary fatigue area. Smaller facets, as in Figure 31(b), was found to have initiated secondary fatigue areas.

Measured sizes of initiation facets are seen in Figure 22. The amount of data points are too small to draw any conclusions but the size of initiation points are comparable to initiation sizes for smooth samples.

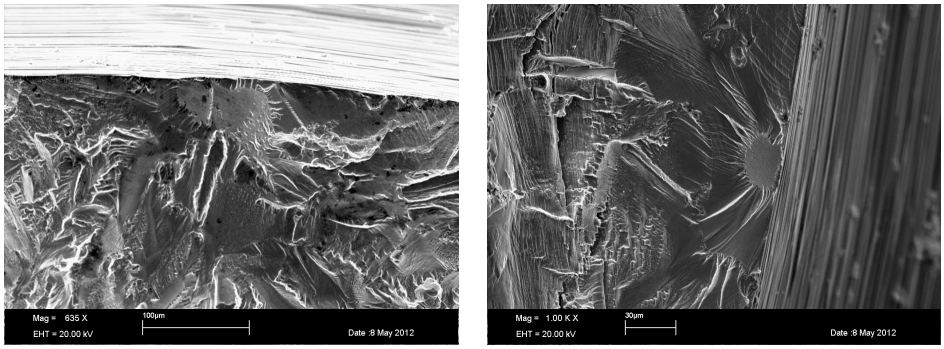

(a) Notched primary initiation (b) Notched secondary initiation

Figure 31: *Two fractographs of surface initiations from one single notched sample tested at high loads, ≥ 5 initiations were clearly visible for this specific sample.* ***a)*** *The primary initiation of $\sim$70x50 μm size.* ***b)*** *A secondary initiation, the appearance is similar but the size differs. In this sample there is a clear correlation between size of initiation and size of fatigue area.*

4.5 Polished cross sections

Polished cross sections from unaffected parts of fatigue samples have also been investigated. The purpose of the investigation was to see if pre-cracked regions or oxide films could be found. The study of notched samples, where initiations were found to be the same facets seen in smooth samples, resulted in the conclusion that the weakness behind the initiation of high temperature samples must be very common. Several initiations of that type was found in the same notched section. The probability is thus high that if the weakness is a pre-cracked defect it should show on a polished cross section.

Two cross sections taken from the thick parts of fatigue samples tested at RT was polished and studied under optical microscope. The cross sections showed no sign of such pre-cracked regions or bifilm oxides.

5 Discussion

As mentioned in the introduction of this report the main goals in this work was to find and measure crack initiations as well as determine the cause of initiation. Of specific interest was to determine if initiations was caused by casting defects as is reported in most articles concerning fatigue properties of cast superalloys. Results have been presented of varying kind in the previous section, they were divided after the kind of investigation performed to acquire the results. This would not suit this section, since it is sometimes necessary to concatenate results from different investigations to draw conclusions. A better suited way to divide this section is to discuss one important topic at a time, regarding all different factors that affect the answer.

5.1 Measured size & location of initiations

Size of initiations have been found to be independent of stress range, the outliers seen in Figure 22 are explained by different initiation mechanisms or large uncertainty in measurement accuracy. Figure 23 shows the correlation between measured size of initiation and total life. There is a good correlation for surface initiations at high temperature, but not so good for surface initiations at RT and internal initiations at high temperature.

The bad correlation for RT samples is most likely connected to difficulties in measuring the size of initiation due to early crack propagation. High temperature internal initiations however were often quite easily distinguished from early crack propagation, but for internal initiations there are many other factors that determine life, most importantly distance from the surface. This is of course expected due to the increased stress concentrations at the surface. A near surface internal defect will quickly reach the surface and become a surface crack where stress intensity is increased. Theoretical calculations predict a stress concentration increase by 55 % for a crack of given size at the surface compare to in the middle of a sample [23].

Notched samples have found to be initiated by smaller facets compared to smooth samples, this could be explained by the following reasoning. Assume that the facets found in high temperature samples are due to a defect of specific size and that they may be assumed to act as a pre-cracked region. Under this premise it would have been an expected result to find smaller initiations for notched samples since the notch reduces the effective area where fatigue will be initiated. Reducing the effective area means reducing the amount of defects where fatigue may be initiated. A reasonable assumption is that the amount of defects are exponentially distributed depending on

their size meaning that the largest defects ($\sim 0.01\,mm^2$) could be quite rare while smaller defects could be more frequently occurring. When notching a smooth sample the probability that a large defect is positioned in the region of high stress concentration is low, but if smaller defects are frequently occurring at least one of these could be found in a region where the stress concentration is high.

A second observation in Figure 22 is the fact that internal initiations are favored at low stress ranges. Under the same premise as above this could also be explained by distribution of defects. At lower stress ranges a large defect is needed to initiate a crack and if the defect of large enough size is rare one might not be found at the surface of the sample. Due to that stress concentrations are higher at the surface a crack initiated at the surface will always grow faster compared to a crack of comparable size initiated internally. If no crack can be initiated at the surface however the internal crack will have no competition. The above argument is however not solid due to the fact that the measured initiations internally seems to be of comparable size to surface initiated cracks. The defects that initiate cracks internally are simply not larger that their surface equals as would have been expected.

The answer to the question could be found in crack propagation rather than initiation. Crack propagation of small cracks is a highly complex area that is not fully understood but it is a well established fact that cracks once initiated does not necessarily have to grow and cause failure. Under some conditions near the threshold value ΔK_{th} small crack propagation may decline and stop entirely. This has been related to a number of different effects such as increased crack closure with increased crack length and crack-tip grain boundary interactions [24]. The cast material investigated in this report has a very large grain size, in orders or mm, it is thus not likely that grain boundary interactions should have a large influence on small crack propagation. Crack closure however has been reported to be substantial in Inconel-718 close to the threshold value ΔK_{th} even at high R-ratios [25]. The article by Yamada & Newman ties the crack closure to debris from contacting surfaces through fretting.

The mode of crack propagation has in this report been noted to differ between internally and surface initiated cracks, internal cracks propagate through stage I crack growth while surface cracks propagate through stage II crack growth. One theory for the preference of internal initiations for low stress ranges could be that crack closure stops crack propagation for surface cracks near the threshold value at low stress ranges. This crack closure would not necessarily affect internal crack propagation and this could cause the preference of internal cracks to cause failure over surface cracks for low stress ranges.

The difficulty of measuring the initiation site may vary greatly between samples. In order to measure a initiation point accurately it is necessary to find distinct differences between initiation and propagation. This is often the case for high temperature samples where initiations are found to be facets and subsequent propagation governed by stage II fatigue. RT samples have been more difficult to classify due to the cleavage-like early crack propagation that is hard to distinguish from initiation features. This difficulty has effected the results in two ways, samples have been found to be unclassifiable and some error has likely been introduced in some cases when measuring initiations in the samples that have been classified. This error is visualized in Figure 23 where there is a small agreement between total life and measured size of initiation for RT samples.

A large number of the facets measured are not aligned parallel to the fracture surface, that is the area of the facet could be larger than what is measured since fractographs are taken from above. This however should not pose a problem since what matters most is how the mode I stress concentration builds up around the defect. This is dependent on the area projected on the plane perpendicular towards the pulling direction, that is the area parallel to the fracture surface. The angle of initiation facets does however enable mode II and mode III loading since shearing forces are introduced. The shearing forces are likely an important factor in some cases of crack propagation. In particular concerning early crack propagation in internally initiated high temperature samples as well as in surface initiated RT samples. This subject is further discussed in the next subsection.

5.2 Crack propagation observations

Crack propagation at RT has been found to be cleavage-like and often coarse close to the initiation site. This has led to some difficulty in determining the size of the initiation point. Typically determination of the initiation point was made difficult by the formation of a large (often in order of mm) straight-cut surface in its vicinity. This kind of surface was inclined at a $\sim 45^\circ$ angle to the fracture plane and had a cleavage like appearance as in Figure 18.

This phenomenon has been reported elsewhere for nickel-base superalloys, for example in an article by Duquette et al. [26] where the formation of a large facet in a single crystal sample was investigated. A model of fatigue cracking has been proposed to explain the formation of large facets, where a combination of shear and tensile forces propagates crack growth. Along the 45° angle shear forces are at maximum, crystallographic planes along this direction are weakened through back and forth slip with every cycle. This

weakening allows tensile forces to crack open the crystallographic plane. This model explains both the crack growth at a large angle toward the fracture plane and the cleavage-like appearance seen on the fracture surface.

The same behavior was not found for high temperature samples. Samples initiated at the surface showed early crack propagation that was typical for stage II fatigue. Samples initiated internally however showed another behavior. Crack propagation was clearly transgranular and along crystal planes forming facets. This behavior has also been reported elsewhere for nickel-base alloys, for example in Kunz et al. [27]. In this report the fatigue properties of nickel-base alloy In-713LC was investigated at high temperature. It was found that early crack propagation from large casting defects was often typical stage I crack propagation, forming facet surfaces.

The general agreement concerning crack propagation modes of nickel-base superalloys is that both stage I and II modes takes place, their occurrence depending on temperature, environment, frequency of loading as well as crack growth rate [28][29]. This report shows that internal contra surface initiations has a large impact on wether stage I or stage II crack propagation takes place. The difference in crack propagation mode of internal contra surface crack growth could of course be related to the different crack growth rates of each crack. An internal crack will feel a smaller stress concentration compared to a surface crack of comparable size and thus it will also grow slower. Another major difference between internal and surface cracks is the environment. Internal cracks will not be affected by the surrounding air which could have a large impact on crack propagation mode.

5.3 Cause of initiation

Previous to this work being conducted it was assumed that the fatigue life of the cast nickel-base alloy would be largely limited by large and easily identified casting defects, such as pores. The main hypothesis to be proven or discarded in this work was that different initiation mechanisms would form different life populations. If this had been found this fact could have been used to improve the accuracy of minimum life predictions from fatigue testing, as described by Jha et al. [30], by only considering the population with minimum life.

Large casting defects has not been found to initiate cracks at any temperature. Initiation sites have been found to be dominated by facet initiations at both RT and high temperature. Only in rare cases has initiation been tied to a deviating initiation mechanism, below sections treat each initiation mechanism separately.

5.3.1 Facet initiations

RT samples have been found to be initiated by facets at the surface of the samples, as in Figure 17. Initiations at high temperature are also dominated by facet features, both internal and formed at the surface, as in Figures 19 and 20(a). The facets found at all temperatures are in the size range of $\sim 40 - 120\ \mu m$. Facets are not generally aligned in a specific angle, such as an angle of high shearing forces as would be the case for slip-plane formed facets. Often they also appear in pairs where one facet can be identified as the crack initiation point. The general appearance of the facets thus points toward that they are some weakness in the structure or even a pre-cracked region where a crack could easily initiate.

In literature the discovery of facets as initiations in cast materials are often regarded to be created through a slip-plane mechanism as described in Section 2.4.1 [27]. Formation of initiation facets through slip-plane mechanisms should however be excluded in this case for mainly two reasons. First, initiation facets found at the surface are not generally aligned in the direction of maximum shear, second, slip-plane mechanisms should not be able to initiate cracks internally in absence of a defect such as a void.

The facet initiations exclude the majority of casting defects often mentioned in literature as crack initiators. The only possible defect mentioned in literature that could cause such initiations are bifilm defects. Double folded oxide films straightened and pinned between growing dendrites could essentially be regarded as a pre-cracked region where cracks could be initiated easily. The findings of features such as the one depicted in Figure 21 was seen as an indication of bifilm presence in the material. EDX analysis and study of polished cross sections was performed mainly in order to investigate the possibility that bifilms are causing the majority of failures.

EDX analysis and fractographic investigations has shown that oxides are often present in the vicinity of the initiation. This could imply that entrained oxides are the main initiation cause, the elemental composition of the oxides however does not support that they should be entrained oxides. Oxides entrained during casting should be rich in elements that are easily oxidized in their melt phase, such as Al, Ti and Cr. The oxides seen on initiation facets at RT does not show increased values of any of these elements. A more likely explanation is that the oxides are from fretting between fracture surfaces during testing.

The fatigue surfaces of high temperature samples are highly oxidized. EDX analysis show that initiation facets are oxidized to a greater extent than the average fatigue surface. This however is also the case for facets formed through stage I crack growth in high temperature samples. It is thus not

likely that the increased oxide content is due to entrained oxide films. Rather the increased oxide content is connected to that these flat surfaces are somehow more easily oxidized. It should be mentioned that a simple EDX analysis is not enough to disprove the existence of bifilm defects since they could potentially be very thin, as thin as a few nanometers [3].

The study of polished cross sections has not resulted in any sign of pre-cracked regions or entrained bifilms in the material. The investigation of notched samples indicated that the defects causing initiation was very common, if these defects were pre-cracked regions due to entrained bifilms several should have been seen on a polished cross section.

In summary it is very difficult to draw conclusions regarding the mechanism behind the initiation of facets at the surface and internally in high temperature samples. It does not seem to be a pre-cracked region, inclusions and shrinkage pores may also be excluded. Rather it seems to be a weakness in the microstructure that is causing initiation and subsequent crack propagation.

5.3.2 Impurity initiations

A few initiations that did not share the appearance of the majority of initiations was found, as in Figure 20(b). EDX analysis showed the brittle initiation area to be rich in Nb. The high amount of Nb in combination with the brittle initiation appearance is an indication that laves phase could be the reason for initiation. Laves phase is an undesirable Tetrahedrally close-packed phase which is commonly present in cast Inconel-718, in this alloy the phase is formed from strong segregation of Nb during solidification. [31]. These laves phases are known to be very brittle [32] and hence one theory for the initiation is that extensive amounts of laves phase has gathered at the initiation, which has lead to an embrittlement of the area. The brittle area is easily cracked once cyclic loads of a large enough amplitude is applied.

The above discussed initiation does not seem to be critical, first of all it is a rare initiation found only in samples from one cast ring. More importantly the total life of samples where this mechanism initiated a crack have been found to be comparable to other internally initiated samples.

5.4 Numerical calculations

The general result of the numerical calculations is that calculated life for RT samples is comparable to actual life, with few exceptions. For high temperature samples the calculated life is approximately a factor of 3 smaller compared to actual life. For HCF samples tested at low stress the calculated life is considerably smaller compared to actual life. This is likely connected to that a long initiation phase is required before crack propagation commences.

Assuming that the numerical calculations were perfectly accurate the results tell us that at RT the initiations measured are completely pre-cracked regions that may be considered as a propagating crack from the very first cycle. For the high temperature samples however the numerical calculations are conservative, calculated life is a factor 3 smaller than actual life. This tells us that an initiation phase leading to the initiation facet measured takes up 75 % of total life while propagation only takes up the remaining 25 %.

Considering that the surface initiations have a similar appearance at both RT and high temperature, and are therefore likely governed by the same initiation mechanism, it would seem that there are some error in the numerical calculations. The result of numerical calculations are of course affected by a number of errors. Mainly three sources of error can be identified, these are initial crack a_i measurement error, model error and crack propagation data scatter.

Fracture mechanics is a well proved and working way of evaluating fatigue life, but it does have some drawbacks. Fracture mechanics perform accurately for large cracks in predicting crack growth for one cycle but the model is not as accurate for smaller cracks, in particular for very small cracks and stress ranges close to the threshold value K_{th}. This non-linear dependence near the threshold value is not considered by linear fracture mechanics which will lead to inaccurate results. The decline in crack rate growth for a small crack as the crack grows has already been discussed previously in Section 5.1. This error is likely the main reason for the general error found in Figure 30.

Propagation data scatter is another error that will have affected the results. Scatter is found both in different crack propagation samples as well as within one sample. For some crack sizes weaknesses will be encountered leading to an accelerated crack growth. The mean data used will hence not be accurate for all samples, in some cases calculated crack growth rates will be higher compared to the actual fatigue samples and in some cases calculated crack growth rates will be slower. This is likely one source of scatter of data in Figures 29 and 30.

6 Conclusion

Samples tested at room temperature are exclusively found to be initiated at the surface. 75 % of samples tested at 650°C are initiated at the surface, 25 % are initiated at a sub-surface location.

Surface initiation sites are in the size range of 40-170 μm. Results from Kitagawa-Takahashi diagrams using $\Delta\sigma_{fl}$ and K_{th} data from fatigue testing at five different temperatures gave a maximum defect size of 190 μm. Internal initiations are favored over surface initiations at low stress range.

Cracks originate from initiation facets in a dominating majority of investigated cases. Facets initiate cracks both at a surface as well as sub-surface location. The mechanism behind the initiation has not been connected to casting defects but evidence that speak against a slip-plane mechanism is presented. Likely is that some weakness in the microstructure initiates cracks. This is an interesting conclusion that is in conflict with the general standpoint of crack initiation in cast Inconel-718, which is that large casting defect initiate crack growth. In two cases were internal initiations connected to another initiation mechanism, embrittlement caused by extensive amount of laves phase.

Crack propagation at 550 and 650°C from fatigue cracks initiated at the surface is typical stage II. Crack propagation at 650°C from fatigue cracks initiated internally is typical crystallographic stage I fatigue, leaving a facet-like propagation surface.

Future work should be focused on determining the cause of initiation in the majority of cases. Knowing the initiation mechanism is very useful when optimizing the microstructure for long fatigue life. Cleaving a facet in half and etching the surface to investigate the microstructure below the facet could be one way to gain a better understanding of the mechanisms initiating cracks. It would especially be interesting to see if the facets are cut in interdendritic regions or through dendrites.

An AUGER investigation could also be an interesting addition to this work. AUGER could be used to investigate the initiating facet surfaces found in RT samples, specifically to investigate wether or not the facet surface is covered in a very thin layer of oxide. AUGER is extremely sensitive in z-direction and together with sputtering it could be used to build a profile of elemental composition in z-direction. If the facet surface is covered by a very thin layer of oxides entrained during casting this investigation should show this. Proof of entrainment during casting would be that the oxide is rich in Al and/or Ti.

References

[1] James L. Handrock Julie A. Bannantine, Jess J. Comer. *Fundamentals of metal fatigue analysis*. Prentice Hall, Englewood Cliffs, N.J., 1990.

[2] F. Alexandre, S. Deyber, and A. Pineau. Modelling the optimum grain size on the low cycle fatigue life of a ni based superalloy in the presence of two possible crack initiation sites. *Scripta Materialia*, 50(1):25 – 30, 2004.

[3] J. Campbell. Entrainment defects. *Materials Science and Technology*, 22(2):127–145, 2006-02-01T00:00:00.

[4] A. Erhard and U. Ewert. *The TOFD Method - Between Radiography and Ultrasonic in Weld Testing*. The German Society for Non-Destructive Testing, May 1999.

[5] Jens Ekengren. *Large and Rare - An extreme values approach to estimating the distribution of large defects in high-performance steels*. PhD thesis, Karlstad University, 2011.

[6] A. de Bussac. *Fatigue & Fracture of Engineering Materials & Structures*, 17:1319, 1994.

[7] S.K. Jha, M.J. Caton, and J.M. Larsen. A new paradigm of fatigue variability behavior and implications for life prediction. *Materials Science and Engineering: A*, 468-470(0):23 – 32, 2007. The McEvily Symposium: Fatigue and Fracture of Traditional and Advanced Materials, TMS 2006.

[8] H. Leon B. Geddes and X. Huang. *Superalloys - Alloying and performance*. ASM International, 2010.

[9] Special Metals Corporation. Material specification inconel alloy 718, September 2007.

[10] Southwest Research Institute. *NASGRO manual 6.1*, July 2010.

[11] Hans Andersson. Hållfasthetslära: Kompendium i utmattning. Chalmers Tekniska Högskola, 1991.

[12] R.W. Hertzberg. *Deformation and fracture mechanics of engineering materials*. John Wiley & Sons, Toronto, third edition edition, 1989.

[13] Charlie R. Brooks and Ashok Choudhury. *Failure analysis of engineering materials*. McGraw-Hill, first edition edition, 2002.

[14] H Andersson, C Persson, and T Hansson. Crack growth in in718 at high temperature. *International Journal of Fatigue*, 23(9):817 – 827, 2001.

[15] H. Andersson and C. Persson. In-situ sem study of fatigue crack growth behaviour in in718. *International Journal of Fatigue*, 26(3):211 – 219, 2004.

[16] J T. Black E. Paul Degarmo and Ronald A. Kohser. *Materials and Processes in Manufacturing*. Wiley, 9th edition edition, 2003.

[17] John Campbell. *Complete casting handbook*. Elsevier Butterworth-Heinemann, 1st edition edition, 2011.

[18] John Campbell. *Castings*. Butterworth-Heinemann, 2nd edition edition, 2003.

[19] N. Green and J. Campbell. *Trans. Am. Found. Soc.*, 102:341–347, 1994.

[20] N. R. Green C. Nyahumwa and J. Campbell. The concept of the fatigue potential of cast alloys. *Journal of the Mechanical Behavior of Materials*, 9(4):227–236, 1998.

[21] N.R. Green J. Campbell, C. Nyahumwa. The concept of the fatigue potential of cast alloys. In *Proceedings of Materials Solution Conference '98 on Advances in Aluminum Casting Technology*, pages 225–233, 1998.

[22] Ludvik Kunz, Petr Lukás, and Radomila Konecna. High-cycle fatigue of ni-base superalloy inconel 713lc. *International Journal of Fatigue*, 32(6):908 – 913, 2010. Selected Papers of the 17th European Conference of Fracture (ECF 17).

[23] D.A. Lados Q.G. Wang, D. Apelian. Fatigue behavior of a356-t6 aluminum cast alloys. part i. effect of casting defects. *Journal of Light Metals*, 1:73–84, 2001.

[24] S. Suresh. *Fatigue of materials*. Cambridge university press, 1st edition edition, 1991.

[25] Y. Yamada and J.C. Newman Jr. Crack closure under high load-ratio conditions for inconel-718 near threshold behavior. *Engineering Fracture Mechanics*, 76(2):209–220, 2009.

[26] M. Gell D. Duquette and J. Piteo. A fractographic study of stage i fatigue cracking in a nickel-base superalloy single crystal. *Metallurgical and Materials Transactions B*, 1(11):3107–3115, 1970.

[27] L. Kunz, P. Lukás, and R. Konecna. Initiation and propagation of fatigue cracks in cast in 713lc superalloy. *Engineering Fracture Mechanics*, 77(11):2008 – 2015, 2010. International Conference on Crack Paths 2009.

[28] J.S. Crompton and J.W. Martin. Crack growth in a single crystal superalloy at elevated temperature. *Metallurgical and Materials Transactions A*, 15:1711–1719, 1984.

[29] J.E. King. Fatigue crack propagation in nickel-base superalloys - effects of microstructure, load ratio and temperature. *Materials Science and Technology*, 3:750–764, 1987.

[30] S.K. Jha, J.M. Larsen, and A.H. Rosenberger. Towards a physics-based description of fatigue variability behavior in probabilistic life-prediction. *Engineering Fracture Mechanics*, 76(5):681 – 694, 2009.

[31] Joel Andersson. *Weldability of Precipitation Hardening Superalloys - Influence of Microstructure*. PhD thesis, Chalmers University of Technology, 2011.

[32] N. S. Stoloff & W. C. Hagel C. T. Sims. *Superalloys II*. John Wiley & Sons, 1987.